

11. SITE 1017¹

Shipboard Scientific Party²

HOLE 1017A

Date occupied: 19 May 1996
Date departed: 19 May 1996
Time on hole: 3 hr, 15 min
Position: 34°32.085'N, 121°6.422'W
Drill pipe measurement from rig floor to seafloor (m): 966.7
Distance between rig floor and sea level (m): 11.1
Water depth (drill pipe measurement from sea level, m): 955.6
Total depth (from rig floor, m): 976.5
Penetration (m): 9.8
Number of cores (including cores having no recovery): 1
Total length of cored section (m): 9.8
Total core recovered (m): 9.9
Core recovery (%): 100.0
Oldest sediment cored:
Depth (mbsf): 9.86
Nature: Clayey silt with foraminifers
Age: Quaternary

HOLE 1017B

Date occupied: 19 May 1996
Date departed: 20 May 1996
Time on hole: 17 hr
Position: 34°32.091'N, 121°6.415'W
Drill pipe measurement from rig floor to seafloor (m): 966.2
Distance between rig floor and sea level (m): 11.1
Water depth (drill pipe measurement from sea level, m): 955.1
Total depth (from rig floor, m): 1170.4
Penetration (m): 204.2
Number of cores (including cores having no recovery): 23
Total length of cored section (m): 204.2
Total core recovered (m): 188.7
Core recovery (%): 92.0
Oldest sediment cored:
Depth (mbsf): 204.2
Nature: Silty clay with diatoms, nannofossil clay
Age: Quaternary

HOLE 1017C

Date occupied: 20 May 1996
Date departed: 21 May 1996
Time on hole: 14 hr, 15 min
Position: 34°32.093'N, 121°6.418'W
Drill pipe measurement from rig floor to seafloor (m): 967.2
Distance between rig floor and sea level (m): 11.1
Water depth (drill pipe measurement from sea level, m): 956.1
Total depth (from rig floor, m): 1141.5
Penetration (m): 174.3
Number of cores (including cores having no recovery): 19
Total length of cored section (m): 174.3
Total core recovered (m): 169.4
Core recovery (%): 97.0
Oldest sediment cored:
Depth (mbsf): 174.3
Nature: Silty clay, nannofossil clay with foraminifers
Age: Quaternary

HOLE 1017D

Date occupied: 21 May 1996
Date departed: 21 May 1996
Time on hole: 9 hr
Position: 34°32.090'N, 121°6.427'W
Drill pipe measurement from rig floor to seafloor (m): 966.4
Distance between rig floor and sea level (m): 11.1
Water depth (drill pipe measurement from sea level, m): 955.3
Total depth (from rig floor, m): 1074.3
Penetration (m): 107.9
Number of cores (including cores having no recovery): 12
Total length of cored section (m): 107.9
Total core recovered (m): 85
Core recovery (%): 78.0
Oldest sediment cored:
Depth (mbsf): 107.9
Nature: Sandy clayey silt
Age: Quaternary

HOLE 1017E

Date occupied: 21 May 1996

¹Lyle, M., Koizumi, I., Richter, C., et al., 1997. *Proc. ODP, Init. Repts.*, 167: College Station, TX (Ocean Drilling Program).

²Shipboard Scientific Party is given in the list preceding the Table of Contents.

Date departed: 21 May 1996

Time on hole: 4 hr, 30 min

Position: 34°32.099'N, 121°6.430'W

Drill pipe measurement from rig floor to seafloor (m): 966.6

Distance between rig floor and sea level (m): 11.1

Water depth (drill pipe measurement from sea level, m): 955.5

Total depth (from rig floor, m): 991.5

Penetration (m): 24.9

Number of cores (including cores having no recovery): 3

Total length of cored section (m): 24.9

Total core recovered (m): 25.7

Core recovery (%): 103.0

Oldest sediment cored:

Depth (mbsf): 24.9

Nature: N/A

Age: Quaternary

Comments: Cores will be split and described postcruise.

Principal results: Site 1017 is located about 50 km west of Point Arguello on the continental slope just south of Santa Lucia Bank at a 955-m water depth. It is the shallow-water drill site in the Conception Transect (35°N). The major objective for drilling was to sample a high-resolution upper Pliocene to Holocene sediment section to compare with ODP Site 893 in the Santa Barbara Basin. Site 1017 is near an important upwelling center off Point Conception and will be important to define the history and cyclicity of upwelling near 35°N. The site will also provide new information about organic carbon diagenesis and about minor element geochemistry through interstitial water profiles and through solid phase analyses.

Five holes were cored with the APC/XCB at Site 1017 (Fig. 1) to a maximum depth of 204.2 mbsf, recovering an apparently continuous interval of Quaternary age (1.2–1.4 to 0.0 Ma). Hole 1017A is a 9.8-m-long failed mudline core. Holes 1017B, 1017C, and 1017D were cored with the APC to refusal and extended with the XCB to depths of 204.2, 174.3, and 107.9 mbsf, respectively. Three APC cores were taken at Hole 1017E down to 24.9 mbsf. Detailed comparisons between the magnetic susceptibility and GRAPE density record generated on the MST, and high-resolution color reflectance measured with the Oregon State University system, showed that a continuous sedimentary sequence may exist down to about 130 mcd. However, exact tie points between adjacent holes could not be established in most cases and precluded the construction of a spliced section.

The sedimentary section begins with ~75 m of greenish gray silty clay to clayey silt and continues downward with 130 m of silty clay to clayey silt and nannofossil clay mixed sediment with minor amounts of foraminifers and diatoms. Thin turbidite layers are a frequent component of the upper two-thirds of the sequence. Cemented dolostone occurs at a few horizons in the lower part of the sequence. Sedimentation rates are around 100–120 m/m.y. on average.

Biostratigraphic age control was provided by calcareous nannofossils and foraminifers (Fig. 1). Diatoms are limited to reworked forms, and radiolarians are absent to rare in the sequence. Changes in planktonic foraminifers indicate strong glacial to interglacial oscillations throughout. Overall, the planktonic foraminifer assemblages reflect relatively cooler conditions than in all earlier drilled sequences of Leg 167. This is likely linked to the location of the site in the heart of the coastal upwelling zone off Point Conception. Other materials observed in the sand-sized sediment fraction include prominent organic debris including fish scales, charcoal fragments, sponge spicules, and echinoid spines. Also observed were large numbers of tar (asphalt) globules that have glued together a variety of biogenic materials, especially sponge spicules. The tar was almost certainly derived from natural oil seeps in the region during the entire Quaternary.

Positive magnetic inclinations in the top 110 mbsf represent most likely the Brunhes Chron. Below the normal polarity interval, the low magnetic intensity and core disturbance by XCB coring precluded the establishment of a magnetic polarity stratigraphy aboard ship.

Carbonate concentrations range between 1 and 22 wt%. At 125 mbsf, an increase in the concentration and fluctuation can be observed. The organic carbon concentration shows a similar increase with depth from average values of ~1.5–2.7 wt% at 170 mbsf. The TOC/TN ratio record displays a remarkably low fluctuation around the average value of 10. Chemical gradients in the interstitial waters reflect organic matter diagenesis, the dissolution of biogenic opal and calcium carbonate, and the influence of authigenic mineral precipitation reactions.

Downhole temperature measurements gave a thermal gradient of 74°C/km. Using an average thermal conductivity of 0.937 W/(m·K) yields a heat-flow estimate of 70 mW/m² at Site 1017.

BACKGROUND AND OBJECTIVES

General Description

Site 1017 is located about 50 km west of Point Arguello on the continental slope, which we have called the Santa Lucia Slope, just south of Santa Lucia Bank (Fig. 2). Water depth at Site 1017 is 955 mbsl. It is the nearshore drill site in the Conception Transect (35°N). The Santa Lucia Slope, which faces southwest, is bounded at its shallow end by the Santa Lucia Bank and at its deep end by Arguello Submarine Canyon. The site was surveyed in detail with the *Maurice Ewing* on cruise EW9504 in 1995 (Lyle et al., 1995a, 1995b; Fig. 3). The intent was to find a thick sediment section above the early Pliocene hiatus noted by Sorlien (1994). Site 1017 penetrated almost to the base of a thick lens of the younger sediments (270 ms TWT, or ~215 mbsf). Drilling was stopped before the hiatus to avoid possible hydrocarbon release.

Site Objectives

Site 1017 was drilled to sample a high-resolution upper Pliocene to Holocene sediment section to compare with Santa Barbara Basin (ODP Site 893). We believed that the Santa Lucia Slope would provide a continuous sedimentary section without interspersed hiatuses. Because Site 1017 is near an important upwelling center off Point Conception (Jones et al., 1983) this site should be important to define the history and cyclicity of upwelling near 35°N. It is ~250 m deeper than the modern oxygen minimum (~700 mbsl). The redox history at this site will be affected by changes in the oxygen minimum depth through time. Waters drawn into Santa Barbara Basin also come from this vicinity and data from Site 1017 should confirm whether Santa Barbara Basin oxygenation is being driven by changes in intermediate water source.

Site 1017 will also provide important new information about organic carbon diagenesis and about minor element geochemistry through interstitial water profiles and through solid phase analyses. Organic carbon contents are moderately high, apparently of dominantly marine origin. Interstitial water sampling, especially within the upper 100 m, will be used to define organic matter oxidation and the removal of oxidants from the interstitial waters and sediments. Organic geochemical analysis will provide data on organic matter preservation in a low oxygen environment.

OPERATIONS

Transit from Site 1016 to Site 1017

The 58.0-nmi transit from Site 1016 to Site 1017 was accomplished in 5.25 hr at an average speed of 11.2 kt. The *JOIDES Resolution* arrived at Site 1017 at 1330 hr on 19 May.

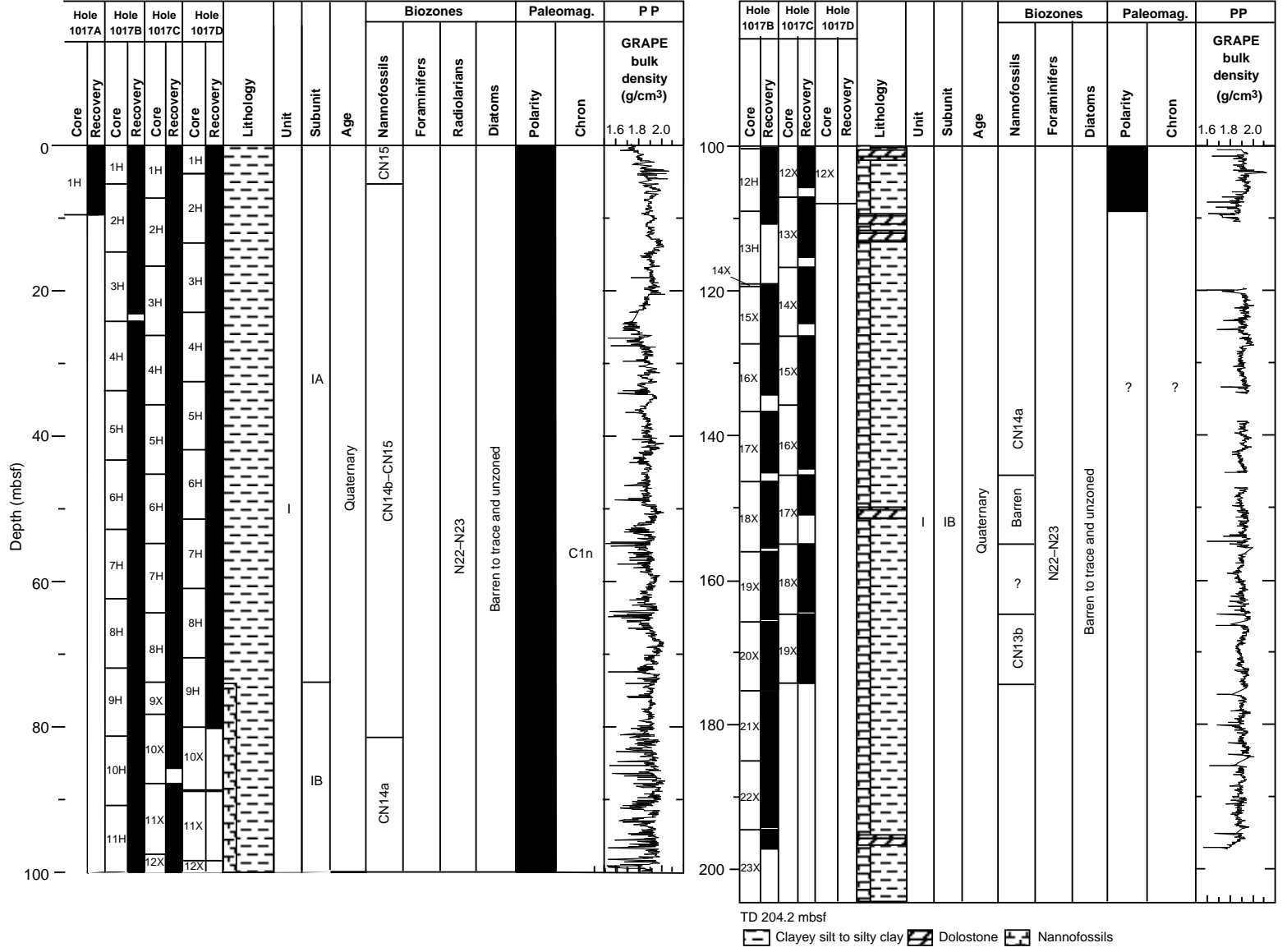


Figure 1. Site 1017 master column.

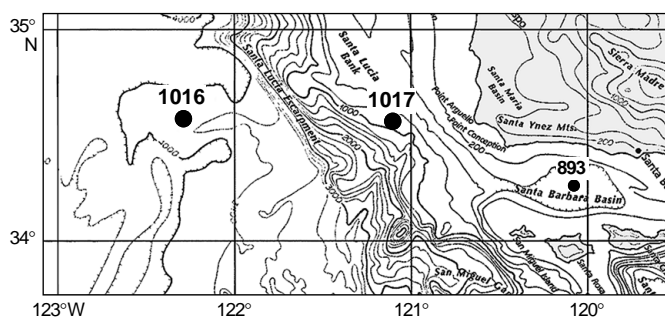


Figure 2. Location map for Site 1017, the nearshore site of the Conception Trench.

Hole 1017A

Hole 1017A was spudded at 1615 hr on 19 May. Core 167-1017A-1H was taken from 0 to 9.5 mbsf with 100% recovery (Table 1; see Table 2 on CD-ROM in the back pocket of this volume for a more detailed coring summary). A full barrel prevented the establishment of an accurate mudline, and the hole was abandoned.

Hole 1017B

The drill pipe was raised 5 m and Hole 1017B was spudded at 1645 hr on 19 May. APC Cores 167-1017B-1H through 13H were taken from 0 to 119.1 mbsf with 96.7% recovery (Table 1). Adara temperature measurements were taken on Cores 167-1017B-4H, 6H, and 8H (see “Physical Properties” section, this chapter). While extracting the core liner following Core 167-1017B-13H, the lower end of the liner fragmented. Safety procedures for handling overpressurized core liners were in place, and no injuries occurred. XCB Cores 167-1017B-14X through 23X were taken down to 204.2 mbsf with 92.4% recovery.

Hole 1017C

The vessel was offset 10 m to the west and Hole 1017C was spudded at 1045 hr on 20 May. APC Cores 167-1017C-1H through 8H were taken from 0 to 73.8 mbsf with 105.2% recovery (Table 1). Oriented cores were obtained starting with Core 167-1017C-3H. XCB Cores 167-1017C-9X through 19X were taken down to 174.3 mbsf with 97.2% recovery. While retrieving Core 167-1017C-14X, the sinker bars hit the crown sheave and parted the coring line. The sinker bars and the oil saver fell to the rig floor. There were no injuries as a result of this incident, but additional safety equipment was installed on the coring winch unit. The winch unit now automatically comes to a complete stop at 10 m below the rig floor and it must be reset in order to continue advancing upward. Coring resumed with the forward coring line.

Hole 1017D

The vessel was offset 10 m to the west and Hole 1017D was spudded at 0045 hr on 21 May. APC Cores 167-1017D-1H through 9H were taken down to 80.1 mbsf with 105.7% recovery (Table 1). XCB Cores 167-1017D-10X through 12X were taken down to 107.9 mbsf with 78.8% recovery.

Hole 1017E

The vessel was offset 10 m to the west and Hole 1017E was spudded at 0945 hr on 21 May. APC Cores 167-1017E-1H through 3H

were taken down to 24.9 mbsf with 103.3% recovery (Table 1). The drill string was tripped back to the surface and secured for the 18-hr transit to Site 1018 by 1330 hr on 21 May.

LITHOSTRATIGRAPHY

Introduction

A lower Quaternary to Holocene (1.2–1.4 to 0.0 Ma) sedimentary sequence was cored at Site 1017. The stratigraphic succession is remarkably uniform from the top to the bottom. The sequence consists almost entirely of silty clay to clayey silt with minor, variable quantities of intermixed foraminifers, nannofossils, and siliciclastic sand (Fig. 4). Disseminated siliciclastic silt and very fine-grained sand are more abundant in the hemipelagic sediment here than at any previous site on Leg 167, except for Site 1015 in Santa Monica Basin. Thin, discrete layers of quartz feldspar or foraminiferal sand are a frequent, volumetrically minor component of the upper two-thirds of the sequence. Cemented dolostone occurs at only a few horizons in the section. Bedding is indistinct, gradational, and very thick (~1 cycle/10 m) until becoming more distinct and thinner (several-meter scale) below about 125 mbsf.

The stratigraphic sequence is grouped into a single lithologic unit with two subunits (Fig. 4), based on visual core descriptions and smear-slide estimates. Unit I consists of a generally homogeneous sequence of clayey silt to silty clay with lesser amounts of nannofossil clay mixed sediment and rare nannofossil ooze. Bedding is generally indistinct in the upper two-thirds, but sharpens and decreases in thickness with increasing depth. The unit is divided into two subunits based on the relative abundance of nannofossils. The contact between the two subunits is approximate because the depth of the lithologic transition is recognized at slightly different depths in the three holes that penetrated it. Subunit IA is composed of silty clay to clayey silt. Subunit IB is composed of silty clay to clayey silt and nannofossil clay mixed sediment, all containing minor amounts of foraminifers and diatoms.

Description of Units

Unit I

Subunit IA

Hole 1017A, Core 167-1017A-1H; 0–9.8 mbsf (base of hole);
 Hole 1017B, interval 167-1017B-1H through 9H-CC; 0–81.3 mbsf;
 Hole 1017C, interval 167-1017C-1H through 8H-CC; 0–73.8 mbsf;
 Hole 1017D, interval 167-1017C-1H through 8H-CC; 0–70.6 mbsf;
 Hole 1017E, interval 167-1017C-1H through 3H-CC; 0–24.9 mbsf
 (base of hole).
 Age: Quaternary, ~0.4 to 0 Ma

Subunit IA is composed of dark olive gray (5Y 3/2) to light grayish olive (10Y 5/2) silty clay to clayey silt, containing minor and variable quantities of foraminifers, nannofossils, and siliciclastic sand. The silt-sized siliciclastic fraction (5% to 60%, mean 30%) is composed of quartz, feldspar, mica, and volcanic glass. Disseminated sponge spicules compose up to 6% of the sediment (mean 2%). Total CaCO₃ content varies from 2% to 14% (see “Organic Geochemistry” section, this chapter). In the fine-grained sediment, smear-slide analyses show that the carbonate is mostly foraminifers (0% to 15%, mean 8%) with rare nannofossils (0% to 8%, mean <2%). Visible organic matter is present in small amounts (TOC = 1% to 2%; see “Organic Geochemistry” section, this chapter) and only a few, scattered macroscopic wood fragments are visible on the split surface of the core. Color, composition, and texture (clay to silt ratio) appears to vary at approximately a 10-m cyclicality. Within thick layers, the sediment is mostly homogeneous. Slight bioturbation is only visible at

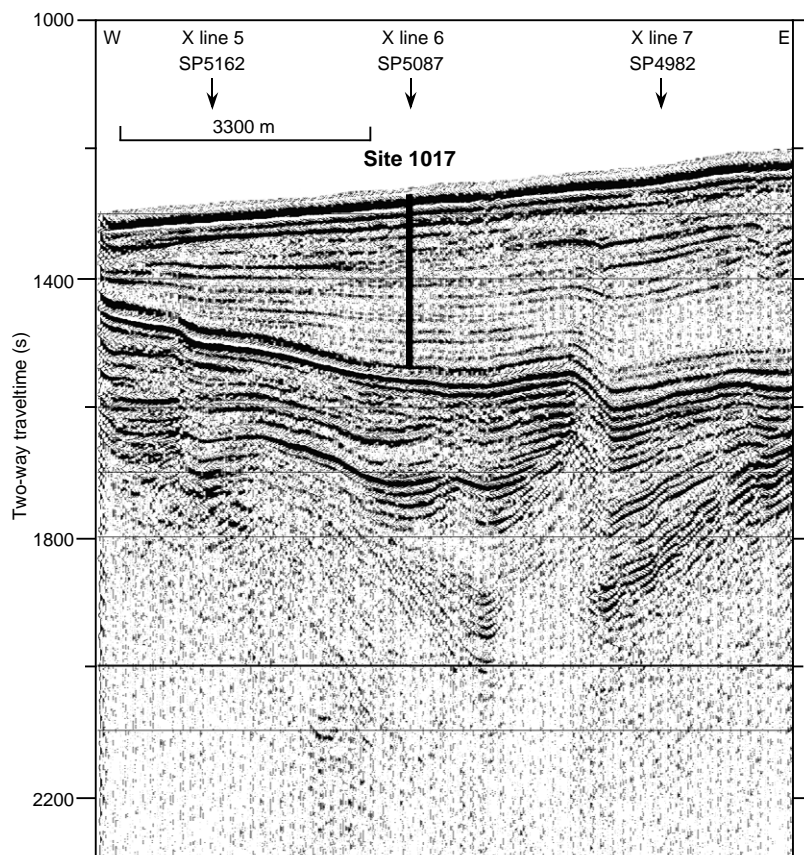


Figure 3. Seismic reflection profile through Site 1017 (line EW9504 CA9-8; Lyle et al., 1995a, 1995b). The summed 4-channel data were filtered between 30 and 200 Hz, with predictive deconvolution and Stolt F-K migration applied. The profile cuts roughly across the Santa Lucia Slope; the prominent reflector just below the maximum depth of Site 1017 was identified before Leg 167 as an early Pliocene hiatus. On y-axis, (s) = milliseconds.

color changes and because of isolated pods of silt or fine-grained sand. Only *Chondrites* trace fossils are identified in this subunit.

Approximately 30 thin, centimeter-scale, quartz-feldspar, macrobioclastic, or foraminiferal sand layers are intercalated with the fine-grained sediment, chiefly between 0–22 mbsf and 60–70 mbsf (Fig. 5). One distinctive dusky red (10R 3/3) sand layer at approximately 3 mbsf is greatly enriched in zircons and other heavy minerals. Amphiboles are present in most sands.

Subunit IB

Hole 1017B, interval 167-1017B-10H-1 through 23X; 81.3–204.2 mbsf (base of hole);

Hole 1017C, interval 167-1017C-9X-1 through 19X; 73.8–174.3 mbsf (base of hole);

Hole 1017D, interval 167-1017C-9H-1 through 12X; 70.6–107.9 mbsf (base of hole).

Age: Quaternary, 1.2–1.4 to ~0.4 Ma

Subunit IB is distinguished from overlying Subunit IA by the presence of relatively nanofossil-rich sediment. The contact between subunits is placed at ~74 mbsf, but was identified at depths ranging from 70.6 to 81.3 mbsf in different holes. Bulk density analyses indicate a small but distinct increase (74 mbsf) corresponding to the increase in nanofossils (see “Physical Properties” section, this chapter).

Subunit IB is composed primarily of very dark gray (5Y 3/1) to light grayish olive (5Y 5/2) silty clay to clayey silt and nanofossil clay mixed sediment. Total carbonate content varies from 2% to ~20% (mean 12%; see “Organic Geochemistry” section, this chapter). Smear-slide analyses show a lesser contribution from foraminifers (0% to 20%, mean 8%) than from nanofossils (0% to 45%, mean ~20%). As in Subunit IA, quartz, feldspar, and volcanic glass make up the silt-sized fraction, but Subunit IB is distinctly siltier

(mean 44%) and sandier overall. Diatoms make up 0% to 10% (mean 4%) of the sediments in this subunit, with radiolarians and silicoflagellates being present in only trace amounts. Sponge spicules are present in nearly all samples, contributing 1% to 10% (mean 4%) of the sediment. There are more macroscopic wood fragments than in Subunit IA, and mean total organic carbon (TOC) nearly doubles below ~160 mbsf (from 1.5% to ~3%; see “Organic Geochemistry” section, this chapter).

Compositional and color variation occurs on a roughly 10-m wavelength until ~125 mbsf. Below ~125 mbsf, color contrast is intensified and occurs on a shorter, meter-scale spacing. Within thick color bands, the sediment is mostly massive, with relatively few distinct burrows. Thin beds and laminations of sand are interbedded within the hemipelagic sediment. The very fine to medium grained, quartz-feldspar sand layers typically have sharp bases, some are graded, and are mainly clustered between 80 and 140 mbsf. In contrast to Subunit IA, amphiboles are absent from these sands. One silty sand deposit at 128 mbsf in Hole 1017B is rich in glauconite and pyrite. Subunit IB also contains five isolated dolostone or dolomitic horizons. Well-indurated, dark olive gray (5Y 3/2) to gray (5Y 5/1) ferroan dolostone beds occur at 115 and 151 mbsf, whereas weakly cemented, olive (5Y 5/3) to pale olive (5Y 6/3) silty dolomitic chalk layers occur at 102, 112, and 197 mbsf. A single, 6-cm diameter, bored dropstone was found within homogeneous clayey silt at 143 mbsf in Hole 1017C.

Depositional History

The sedimentary sequence at Site 1017 records Quaternary hemipelagic accumulation of fine-grained terrigenous sediments on the relatively proximal Santa Lucia slope. Marine biogenous material, especially foraminifers and calcareous nanofossils, is a persistent,

Table 1. Coring summary for Site 1017.

Core	Date (May 1996)	Time	Top (mbsf)	Bottom (mbsf)	Length cored (m)	Length recovered (m)	Recovery (%)
167-1017A-1H	19	2330	0.0	9.8	9.8	9.86	100.0
167-1017B-1H	19	2355	0.0	5.3	5.3	5.25	99.0
2H	20	0025	5.3	14.8	9.5	9.95	105.0
3H	20	0045	14.8	24.3	9.5	8.63	90.8
4H	20	0125	24.3	33.8	9.5	10.23	107.7
5H	20	0145	33.8	43.3	9.5	10.09	106.2
6H	20	0225	43.3	52.8	9.5	10.30	108.4
7H	20	0245	52.8	62.3	9.5	10.04	105.7
8H	20	0320	62.3	71.8	9.5	10.56	111.1
9H	20	0355	71.8	81.3	9.5	10.04	105.7
10H	20	0425	81.3	90.8	9.5	10.04	105.7
11H	20	0445	90.8	100.3	9.5	9.71	102.0
12H	20	0510	100.3	109.8	9.5	10.00	105.2
13H	20	0550	109.8	119.1	9.3	0.28	3.0
14X	20	0800	119.1	119.3	0.2	0.17	85.0
15X	20	0835	119.3	127.3	8.0	8.43	105.0
16X	20	0915	127.3	136.8	9.5	6.98	73.5
17X	20	1005	136.8	146.5	9.7	8.42	86.8
18X	20	1045	146.5	156.1	9.6	9.11	94.9
19X	20	1145	156.1	165.8	9.7	9.55	98.4
20X	20	1230	165.8	175.4	9.6	9.52	99.1
21X	20	1330	175.4	185.0	9.6	9.37	97.6
22X	20	1425	185.0	194.6	9.6	9.44	98.3
23X	20	1545	194.6	204.2	9.6	2.63	27.4
167-1017C-1H	20	1750	0.0	7.3	7.3	7.30	100.0
2H	20	1820	7.3	16.8	9.5	9.90	104.0
3H	20	1900	16.8	26.3	9.5	10.06	105.9
4H	20	1920	26.3	35.8	9.5	10.10	106.3
5H	20	1945	35.8	45.3	9.5	10.26	108.0
6H	20	2005	45.3	54.8	9.5	10.15	106.8
7H	20	2030	54.8	64.3	9.5	9.73	102.0
8H	20	2100	64.3	73.8	9.5	10.12	106.5
9X	20	2210	73.8	78.3	4.5	7.50	166.0
10X	20	2240	78.3	87.9	9.6	7.39	77.0
11X	20	2300	87.9	97.5	9.6	9.38	97.7
12X	20	2330	97.5	107.1	9.6	8.37	87.2
13X	21	0000	107.1	116.8	9.7	8.25	85.0
14X	21	0030	116.8	126.4	9.6	7.84	81.6
15X	21	0300	126.4	135.9	9.5	9.59	101.0
16X	21	0345	135.9	145.5	9.6	8.69	90.5
17X	21	0435	145.5	155.1	9.6	5.58	58.1
18X	21	0515	155.1	164.7	9.6	9.39	97.8
19X	21	0555	164.7	174.3	9.6	9.77	102.0
167-1017D-1H	21	0750	0.0	4.1	4.1	4.10	100.0
2H	21	0830	4.1	13.6	9.5	9.97	105.0
3H	21	0855	13.6	23.1	9.5	9.64	101.0
4H	21	0930	23.1	32.6	9.5	10.04	105.7
5H	21	1000	32.6	42.1	9.5	10.12	106.5
6H	21	1030	42.1	51.6	9.5	10.32	108.6
7H	21	1105	51.6	61.1	9.5	9.83	103.0
8H	21	1135	61.1	70.6	9.5	10.43	109.8
9H	21	1205	70.6	80.1	9.5	10.25	107.9
10X	21	1320	80.1	88.7	8.6	0.17	2.0
11X	21	1400	88.7	98.3	9.6	0.05	0.5
12X	21	1500	98.3	107.9	9.6	0.09	0.9
167-1017E-1H	21	1650	0.0	5.9	5.9	5.91	100.0
2H	21	1720	5.9	15.4	9.5	10.06	105.9
3H	21	1745	15.4	24.9	9.5	9.74	102.0

Note: Table 2, on the CD-ROM in the back pocket, this volume, is a more detailed coring summary.

though minor, sedimentary component. Continuous hemipelagic sedimentation was infrequently interrupted by deposition of thin silty to sandy turbidites. Cyclic variation in texture and composition changed in both periodicity and magnitude through the sequence.

The calcareous silty clay and clayey silt of Subunit IB accumulated at ~105 m/m.y. from the early to late Quaternary (~1.4 to 0.4 Ma; see "Biostratigraphy" section, this chapter). A large dolomite dropstone characteristic of the Miocene Monterey Formation outcrops along the central Californian coast was deposited at ~0.9 Ma. Pholadidae clam borings indicate that the dropstone had been in the near-shore environment, where it likely served as an anchor for a kelp holdfast that eventually carried it offshore. Deposition of sand and silt by turbidity currents became frequent between ~1.0 and 0.5 Ma,

possibly reflecting Quaternary tectonic compression and uplift of the adjacent Santa Lucia Bank (Sorlien, 1994). Five dolostone or dolomitic horizons reflect early carbonate diagenesis in a relatively organic-rich environment, possibly associated with brief pauses in sedimentation (Middelburg et al., 1990). Meter-scale cyclic alternation in the siliciclastic and carbonate composition of the lower part of the section reflects variation with a period of tens of thousands of years. At ~0.9 Ma, compositional oscillation slowed to approximately 100-k.y.-scale periodicity.

Sedimentation accelerated to ~188 m/m.y. during late Quaternary (~0.4 to 0 Ma; see "Biostratigraphy" section, this chapter) deposition of the silty clay and clayey silt of Subunit IA. The corresponding decrease in carbonate content compared with the early Quaternary sed-

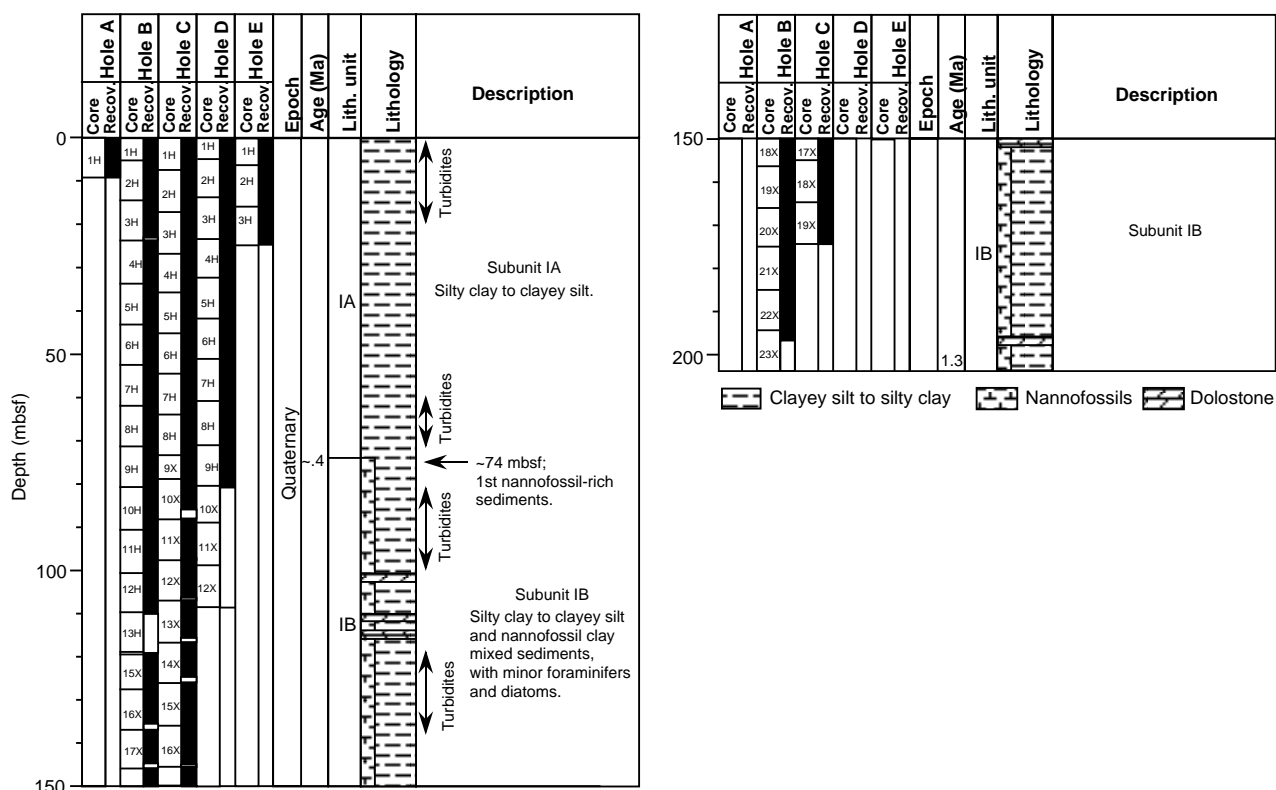


Figure 4. Site 1017 lithostratigraphic summary (0–204.2 mbsf).

iments reflects the dilution of carbonate accumulation by the increased rate of siliciclastic sedimentation. Deposition of thin siliciclastic and foraminiferal sand turbidites occurred relatively frequently at ~0.4 Ma and during the past 100 k.y. as the overall rate of sedimentation increased.

BIOSTRATIGRAPHY

The five holes at Site 1017 recovered an apparently continuous sediment sequence of the Quaternary. The base of Hole 1017C, dated using calcareous nannofossils, is between 1.2 and 1.4 Ma in age (Fig. 6).

Calcareous nannofossils are of highly variable abundance and quality of preservation throughout the sequence. The section above 175 mbsf is marked by mostly abundant to common and well-preserved planktonic and benthic foraminifers. Below 175 mbsf to the base of Hole 1017B at 204 mbsf, the section is essentially barren of planktonic foraminifers and benthic foraminifers are either absent or occur in low abundances. Diatoms are almost exclusively limited to reworked forms and radiolarians are absent to rare in the sequence.

Changes in planktonic foraminifers indicate strong glacial to interglacial oscillations throughout. Overall, both interglacial and glacial planktonic foraminifer assemblages reflect relatively cooler conditions than in all earlier drilled sequences of Leg 167. This is almost certainly because of Site 1017's location in the heart of the coastal upwelling zone off Point Conception. Planktonic foraminifer assemblages younger than ~700 to 800 ka contain populations of *Neogloboquadrina pachyderma* more strongly dominated by sinistrally coiled forms compared with older assemblages. This change towards inferred cooler conditions appears to correlate with a well-known cooling step at ~800 ka during the late Quaternary, associated with Northern Hemisphere cryosphere development (Pisias et al., 1995).

Benthic foraminifer assemblages exhibit large differences between glacial and interglacial episodes. Assemblages associated with typical glacial planktonic foraminifer faunas reflect relatively higher oxygen concentrations of bottom waters, while those associated with interglacial faunas reflect distinctly lower oxygen concentrations in bottom waters, as in Santa Barbara and Tanner Basins.

Planktonic Foraminifers

Site 1017 contains an excellent and apparently continuous sequence of planktonic and benthic foraminifers of Quaternary age from 175 mbsf (Sample 167-1017B-20X-CC) to the top of the section (Tables 3, 4). In this part of the sequence, both planktonic and benthic foraminifers are mostly abundant to common and of good preservation. Below 175 mbsf to the base of the Hole at 204 mbsf, the section is essentially barren of planktonic foraminifers and benthic foraminifers are either absent or occur in low abundances.

The distribution of most planktonic foraminifer species is strongly controlled by surface-water temperature changes associated with glacial/interglacial oscillations. Glacial assemblages are dominated by *N. pachyderma* (sinistral) and *Globigerina bulloides* and exhibit very low diversity. Interglacial assemblages are dominated by *N. pachyderma* (dextral) and *G. bulloides*, exhibit higher diversity, and include forms such as *Neogloboquadrina dutertrei* or *N. humerosa* and *Globorotalia inflata*. The planktonic foraminifers at Site 1017 reflect cooler conditions during the Quaternary compared with earlier sites drilled during Leg 167, almost certainly because of its location in the region of strong upwelling off Point Conception. Because of the cooler conditions, interglacial assemblages contain fewer species compared with sites to the south in the California Borderland. Also, glacial assemblages contain *N. pachyderma* populations with very high percentages of sinistrally coiled forms (Tables 3, 4). Most core-catcher samples above 137 mbsf in Hole 1017B (above Sample 167-1017B-16X-CC; Table 3) and above 107 mbsf in Hole 1017C (above

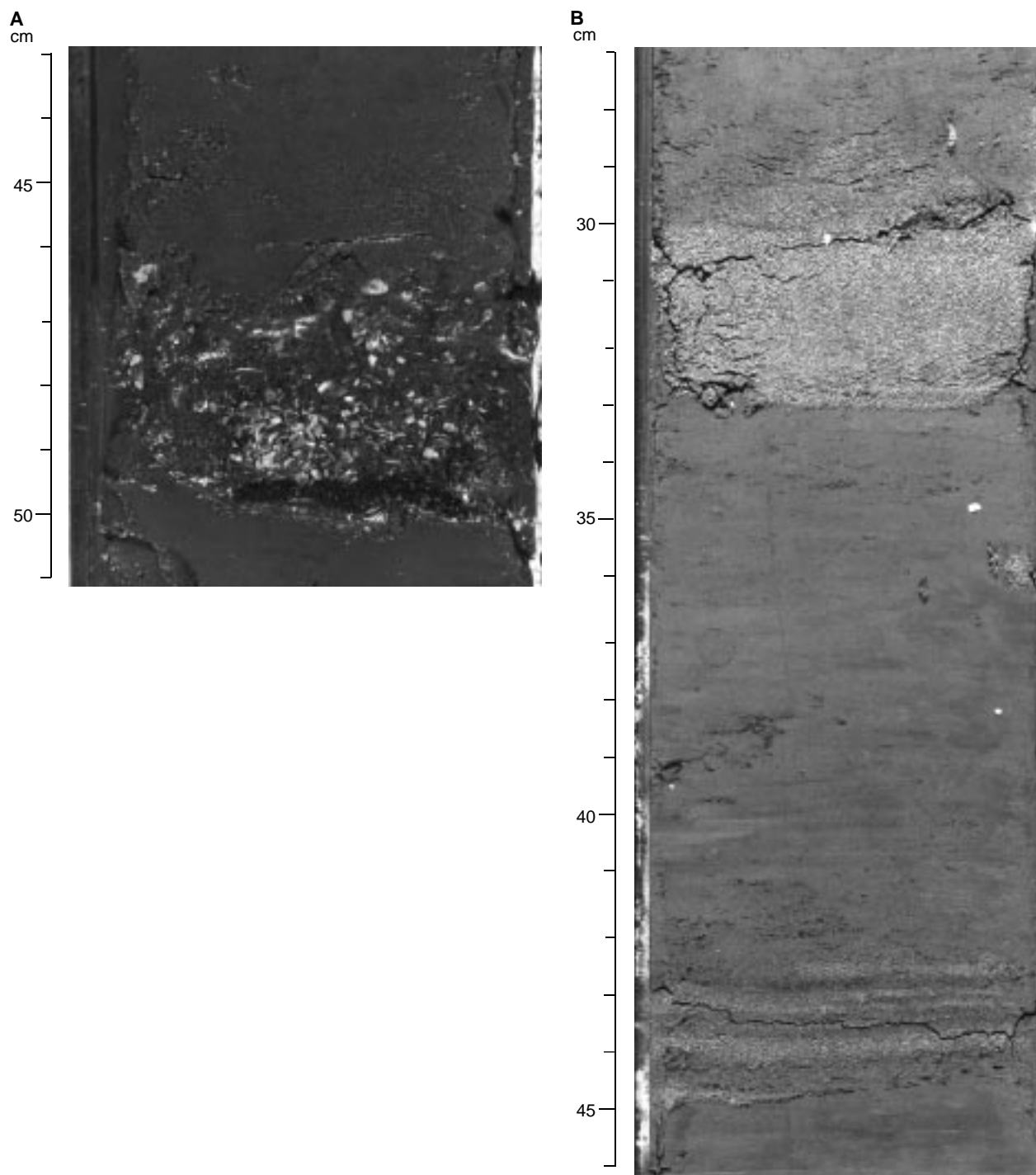


Figure 5. Sand turbidites at Site 1017. **A.** Bioclastic sand, interval 1017A-1H-2, 43–51 cm. **B.** Quartz-feldspar sand deposits, interval 1017B-10H-4, 27–46 cm.

Sample 167-1017C-12X-CC; Table 4) exhibit *N. pachyderma* populations strongly dominated by sinistrally coiled forms compared with the sequence below. This level has been dated using calcareous nanofossils to be between ~700 and 800 ka and may reflect a well-known cooling step during the late Quaternary (~800 ka) associated with northern hemisphere glacial development.

The few potential planktonic foraminifer datums at Site 1017 are strongly diachronous compared with sites to the south. This diachronism probably resulted from the significantly cooler conditions at

Site 1017 related to strong upwelling. *N. dutertrei* first appeared at 220 ka (Sample 167-1017B-5H-CC) compared to 1.0 Ma at Leg 167 sites to the south. The LO of *N. humerosa* was also much later at 360 ka (Sample 167-1017B-9H-CC) compared with 1.2 Ma at sites to the south.

Benthic foraminifers are usually abundant, diverse, and very well preserved. The assemblages exhibit little dissolution throughout the middle and late Quaternary. Benthic foraminifer assemblages exhibit large differences between glacial and interglacial episodes, as de-

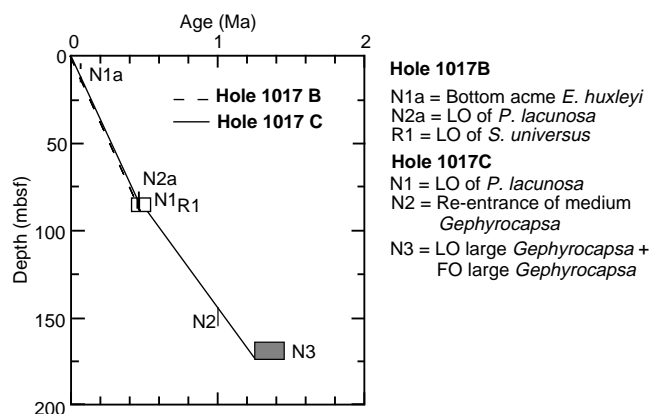


Figure 6. Age/depth plot for Holes 1017B and 1017C.

fined by planktonic foraminifer assemblages. Assemblages associated with glacial episodes are often dominated by *Uvigerina* and contain a number of other taxa in variable proportions including *Bulimina spicata*, *Globobulimina pacifica*, *Bolivina argentea*, *B. pseudobeyrichi*, *Cassidulina delicata*, *Buliminella tenuata*, *Epistominella smithi*, *Hoeglundina elegans*, *Oridorsalis tenera*, *Eponides umbonatus*, *Valvulinera* spp., and *Cibicidoides* spp. Interglacial assemblages exhibit much lower diversity and are dominated instead by species of *Bolivina* and include other taxa such as *Uvigerina*, *Buliminella*, and *Globobulimina*. This assemblage reflects relatively higher oxygen concentrations of bottom waters during glacial episodes and lower concentrations during interglacial episodes. Reworking of pre-Quaternary benthic and planktonic foraminifers is not common. However, local reworking of Quaternary foraminifers may be important, as suggested by the presence of foraminifer sands in some core intervals (for example, Sample 167-1017C-7H-CC), almost completely dominated by a single taxon such as *Uvigerina*. Such reworking is difficult to detect because of the excellent preservation of most of the specimens.

Other materials observed in the sand-sized fraction of many of the core-catcher samples include prominent fish remains, charcoal fragments, sponge spicules, and echinoid spines. Also observed were large numbers of tar (asphalt) globules that have glued together a variety of biogenic materials, especially sponge spicules. The tar was almost certainly derived from natural oil seeps in the region during the entire Quaternary.

Calcareous Nannofossils

Calcareous nannofossils are absent to abundant and poorly to well preserved in Holes 1017B and 1017C (Table 5). The sequence spans an interval from the lower Pleistocene Zone CN13b to the Holocene Zone CN15.

Calcareous nannofossil assemblages are marked by the presence of *Emiliania huxleyi*, *Pseudoemiliania lacunosa*, *Calcidiscus leptoporus*, *Helicosphaera carteri*, *Helicosphaera sellii*, and several morphotypes of *Gephyrocapsa* spp. and *Ceratolithoides*.

The expanded Quaternary sequence at Site 1017 allows recognition of the base of the acme of *E. huxleyi* in the latest Pleistocene (85 ka) at 5.3 mbsf (Sample 167-1017B-1H-CC) and the top of *P. lacunosa* (460 ka) at 90.80 mbsf (Sample 167-1017B-10H-CC). In Hole 1017C, the presence of large *Gephyrocapsa* at 174.30 mbsf (Sample 167-1017C-19X-CC) allows assignment of an early Pleistocene age to this sample. Reworked Miocene and Oligocene calcareous nannofossils are persistent throughout the sequence but are never important components in the assemblages.

Diatoms

Site 1017 exhibits a characteristic biosiliceous component made up of trace amounts of fragmented diatoms, rare reworked diatoms of middle Miocene age, and common fresh sponge spicules. Thus, Site 1017 is similar to Sites 1012, 1013, and 1014. These mixtures suggest a persistence of reworking of relatively shallow-water components during the late Neogene. Although sparse occurrences are documented of *Actinocyclus oculatus* in Sample 167-1017B-11H-CC and of *Simonseniella (Rhizosolenia) curvirostris* in Sample 167-1017B-12H-CC (Table 6), diatom biostratigraphy is ineffective at Site 1017.

Radiolarians

Radiolarians are absent to rare and moderately to well preserved in core catchers at Hole 1017B (Table 7). Because of the scarcity of Arctic assemblages, no radiolarian event could be recognized. The interval above Sample 167-1017B-9H-CC (81.3 mbsf) is tentatively placed in the upper Quaternary *Botryostrobus aquilonaris* Zone. The occurrence of very rare and broken representatives of *Eucyrtidium matuyamai* places the lower part of the hole (175.4 to 194.6 mbsf) in the upper Pliocene to lower Quaternary *E. matuyamai* Zone (1 to 2 Ma).

PALEOMAGNETISM

We made magnetic measurements on the archive halves of 12 APC cores and a few XCB cores from Hole 1017B with the pass-through cryogenic magnetometer. After measuring the natural remanent magnetization (NRM) the sections were demagnetized with a peak alternating field (AF) of 15 mT. The NRM intensity ranged between 3 and 10 mA/m; after AF cleaning it was reduced to values between 0.5 and 3 mA/m (Fig. 7). After AF treatment the magnetization of most sections was just above the sensitivity limit of the magnetometer (>0.7 mA/m). There was no interval of negative inclination (reverse polarity) in Hole 1017B, except for Section 167-1017B-15X-5. Quite likely the positive inclinations of the top 110 mbsf of Hole 1017B represent Chron C1n (Brunhes).

Based on nannofossil biostratigraphic data the last appearance datum of large *Gephyrocapsa* spp., dated at about 1.2 Ma, occurs in Core 167-1017C-19X (see "Biostratigraphy" section, this chapter). In an attempt to find the Matuyama reverse polarity interval, we measured the best-preserved sections of each XCB core from Hole 1017C using AF demagnetization at 15 and 25 mT. Unfortunately, the magnetization of most sections was lower than the sensitivity of the magnetometer after AF demagnetization (Fig. 8). Demagnetization of the XCB cores from Hole 1017C did not reveal an interval with negative inclinations (reverse polarity). Below the APC cored interval of normal polarity (0–109.8 mbsf), an interpretation of the inclination record was not possible because of the low magnetic intensity and core disturbance by XCB drilling.

COMPOSITE DEPTHS AND SEDIMENTATION RATES

Multisensor track (MST) data collected at 4-cm intervals from Holes 1017A through 1017E, and color reflectance data collected at 6- to 10-cm intervals from Holes 1017B, 1017C, and 1017D were used to determine depth offsets in the composite section. On the composite depth scale (expressed as mcd, meters composite depth), features of the plotted MST and color reflectance data present in adjacent holes are aligned so that they occur at approximately the same depth. Working from the top of the sedimentary sequence, a constant was added to the mbsf (meters below sea floor) depth for each core

Table 3. Distribution and relative abundances of planktonic foraminifers in Hole 1017B.

Zone	Core, section, interval	Depth (mbsf)	Abundance	Preservation	<i>Globorotalia inflata</i>	<i>Neogloboquadrina duterrei</i>	<i>Neogloboquadrina humerosa</i>	<i>Neogloboquadrina cf. kagaensis</i>	<i>Neogloboquadrina pachyderma</i> dex.	<i>Neogloboquadrina pachyderma</i> sin.	<i>Globigerina bulloides</i>	<i>Orbulina universa</i>	<i>Globigerinoides ruber</i>	<i>Globorotalia scitula</i>	<i>Hastigerina aequilateralis</i>	<i>Globigerina umbilicata</i>	<i>Globigerina apertura</i>	<i>Globigerina quinqueloba</i>	<i>Globigerinita glutinata</i>	<i>Globorotalia truncatulinoides</i>	<i>Globigerina falcomensis</i>
N22/23	167-1017B-1H-CC	5	A	G						A	A	R		C							
	2H-CC	15	C	G						A	A	R		C							
	3H-CC	24	A	G	F	A			A	A	A	C	R		F					R	R
	4H-CC	34	C	G						A	A	C									
	5H-CC	43	A	G			C		A	A	C	F	R								
	6H-CC	53	A	G						A	A	A									
	7H-CC	62	A	G	R					A	A	A	R			A					
	8H-CC	71	C	G						A	A	F									
	9H-CC	81	A	G	F		F		A	A	A	F	R	R		C		A			
	10H-CC	91	C	G						A	A	C	R					C			
	11X-CC	100	A	G	F		C			A	A	A		R				A		R	
	12X-CC	110	A	G						A	A	A				A					
	13X-CC	119	C	M					F	A	A	A									
	14X-CC	NCC								A	A	A									
	15X-CC	127	A	G				A		A	A	A						C		C	
	16X-CC	137	A	M	C				C	A	A	R									
	17X-CC	147	A	G	R			A	A	A	A										
	18X-CC	156	C	M	R				A	A	A										
	19X-CC	166	R	P					C	A	A	R									
	20X-CC	175	F	M						C	F	R									
	21X-CC	185	P																		
	22X-CC	194	B																		
	23X-CC	204	B																		

Notes: See "Explanatory Notes" chapter for abbreviations. NCC = no core catcher.

Table 4. Coiling dominance of *Neogloboquadrina pachyderma* in Hole 1017C.

Core, section, interval	Depth (mbsf)	<i>Neogloboquadrina pachyderma</i> coiling dominance
167-1017C-1H-CC	7	Sinistral
2H-CC	17	Sinistral
3H-CC	26	Sinistral
4H-CC	36	Sinistral
5H-CC	45	Sinistral
6H-CC	55	Sinistral
7H-CC	64	Sinistral
8H-CC	74	Sinistral
9X-CC	78	Sinistral
10X-CC	87	Sinistral
11X-CC	98	Sinistral
12X-CC	107	Sinistral
13X-CC	117	Sinistral/Dextral
14X-CC	126	Sinistral/Dextral
15X-CC	136	Sinistral/Dextral
16X-CC	146	Sinistral/Dextral
17X-CC	155	No core catcher
18X-CC	165	Sinistral/Dextral
19X-CC	174	Sinistral

in each hole to arrive at a mcd depth for that core. The depths offsets that compose the composite depth section are given in Table 8 (also on CD-ROM, back pocket). Because it was difficult to distinguish features in the MST and color reflectance data that could be correlated across adjacent holes, continuity of the sedimentary sequence is difficult to verify. A continuous sedimentary sequence may exist down to about 130 mcd, but exact tie points between adjacent holes could not be made in most cases. Below 130 mcd, cores from Holes 1017B and 1017C do not always overlap (Fig. 9; e.g., see intervals around 153 mcd, 164 mcd, and 185 mcd).

Color reflectance measurements were the primary parameters used for interhole correlation purposes. Magnetic susceptibility and GRAPE measurements were used in a few intervals to provide additional support for composite construction although, in general, these measurements were not as useful because of the low variability of the signal. Natural gamma-ray activity measurements were made throughout the entire section in Holes 1017A through 1017C, but the sampling interval of 12 cm was insufficient for interhole correlations.

The color reflectance, GRAPE, and magnetic susceptibility records used to correlate between holes for Site 1017 are shown on a composite depth scale in Figures 9, 10, and 11, respectively. The GRAPE data were used to identify intervals of voids and highly disturbed sediments (values less than 1.45 g/cm³) and all MST and color reflectance data from these intervals were culled. The composite records suggest that up to 3 m of material may be missing between cores down to about 130 mcd, although the average gap is less than one meter. As there are no data to fill possible core gaps below 130 mcd, an assessment of core gap length below this depth is not possible.

A preliminary age model was constructed for Site 1017, and sedimentation rates are shown in Table 9. As there are only three control points, this age model provides only a rough estimate of sedimentation rates at this site.

INORGANIC GEOCHEMISTRY

We collected 12 interstitial water samples from Site 1017, one from Hole 1017A at 5.67 mbsf and 11 from Hole 1017B at depths ranging from 4.45 to 179.85 mbsf. For the purposes of this report, these are treated as constituting a single profile. Chemical gradients in the interstitial waters at this site (Table 10) reflect organic matter

Table 5. Distribution and relative abundances of calcareous nannofossils in Holes 1017A, 1017B, and 1017C.

Zone	Core, section, interval	Depth (mbsf)	Preservation	Abundance	<i>Emiliania huxleyi</i>	<i>Pseudoemiliania lacunosa</i>	<i>Helicosphaera carteri</i>	<i>Helicosphaera sellii</i>	<i>Gephyrocapsa oceanica</i> s.l.	<i>Gephyrocapsa</i> sp. 3	<i>Gephyrocapsa</i> small	<i>Gephyrocapsa</i> large	<i>Ceratolithus telesmus</i>	<i>Coccolithus pelagicus</i>	<i>Calcidiscus macintyreii</i> > 11 µm	<i>Calcidiscus leptoporus</i>
CN15–CN14b	167-1017A-1H-CC	9.8	M	F/C			R		R		C			F		R
	167-1017B-1H-CC	5.3	M/G	C	P						C			F		R
CN15–CN14b	2H-CC	14.8	M	A			R				A			F		R
CN15–CN14b	3H-CC	24.3	M	A	?		R		C	F	A	R	R	C		R
CN15–CN14b	4H-CC	33.8		B												
CN15–CN14b	5H-CC	43.3	G	A			C		C				R			C
CN15–CN14b	6H-CC	52.8	M/G	F/C							A			P		R
CN15–CN14b	7H-CC	62.3	M	C					C		A					R
CN15–CN14b	8H-CC	71.8	P	F/C			R		R		P					R
CN15–CN14b	9H-CC	81.3	G	C/A					C/F		A			F		R
CN14a?	10H-CC	90.8	P	F		RR			P		P			P		R
CN14a	11H-CC	100.3	M	F/C		R	R		R							R
	12H-CC	109.8		B												
CN14a?	13H-CC	119.1	P	RR		P										R
CN14a–CN13b	15X-CC	127.3	G	A		C				D				F		R
CN14a–CN13b	16X-CC	136.8	M	C		P	F		RR	A						R
CN14a–CN13b	17X-CC	146.5	M/G	A		F/C				D						R
CN14a–CN13b	18X-CC	156.1	P	R		P	R							C		R
CN14a–CN13b	19X-CC	165.8	P	R/F		P				P						P
	20X-CC	175.4		B												
CN14a–CN13b	21X-CC	185.0	M	A		P			C	A						R
	22X-CC	194.6	P	R		P								R		R
	23X-CC	204.2		B												
	167-1017C-1H-CC	7.3	M/G	A	P				R		A			P		R/F
CN15–CN14b	2H-CC	16.8	P	R							C			C		
CN15–CN14b	3H-CC	26.3	M	C/A			R/F		P	R	A					
	4H-CC	35.8		B												
CN15–CN14b	5H-CC	45.3	M/G	A			F		C		A			P		
CN15–CN14b	6H-CC	54.8	P	RR						P						
CN15–CN14b	7H-CC	64.3	G	F/C			R		C		A					
CN15–CN14b	8H-CC	73.8	M	A			F		P		P					R
CN15–CN14b	9X-CC	78.3	G	A					C		A			P		R
CN14a	10X-CC	87.3	P	F/C		F			R		C					R
CN14a	11X-CC	97.5	G	A		RR	R		P	RR	A					R
CN14a	12X-CC	107.1	G	M/A		C			R		A			P		C
	13X-CC	116.8	M	RR		P										
	14X-CC	126.4	G	A		C	R				A			R		R
CN14a	15X-CC	135.9	G	A		F			R/F	D						R
CN14a	16X-CC	145.5	G	A		C	R		P	C	A			P		R
	17X-CC	155.1		B												
	18X-CC	164.7	M	C		P										
CN13b	19X-CC	174.3	P	R/F		P		P			R			P		R

Note: See “Explanatory Notes” chapter for abbreviations.

diagenesis, the dissolution of biogenic opal and calcium carbonate, and the influence of authigenic mineral precipitation.

Chlorinity ranges from 549 to 556 mM from 4.45 to 47.75 mbsf, then decreases slightly to values of 545–548 mM from 76.25 to 179.85 mbsf (Fig. 12). Salinity, measured refractively as total dissolved solids, ranges from 32 to 36. Sodium concentrations measured by flame emission spectrophotometry were on average <4% lower than those estimated by charge balance (Table 10).

Alkalinity increases to peak values >40 mM from 19.25 to 47.75 mbsf, then decreases to an average of 34 mM from 76.25 to 179.85 mbsf (Fig. 12). Sulfate concentrations decrease to values below the detection limit (approximately 1.4 mM) by 19.25 mbsf. Phosphate concentrations increase to values >100 µM from 9.75 to 47.75 mbsf, with a peak value of 161 µM at 19.25 mbsf near the depth where sulfate goes to zero, and alkalinity increases to near its maximum value, then decreases with increasing depth to 12 µM by 179.85 mbsf. Ammonium concentrations increase with increasing depth to an average of 8.5 mM from 76.25 to 179.85 mbsf. Dissolved manganese concentrations are below the detection limit (2 µM) in all samples.

Dissolved silicate concentrations increase with depth, at first rapidly, then more slowly, to values averaging 960 µM from 76.25 to 179.85 mbsf (Fig. 12), indicative of the dissolution of biogenic opal. Strontium concentrations are around seawater values in the upper 75 m, equivalent to lithostratigraphic Subunit IA (see “Lithostratigraphy” section, this chapter), then increase with depth to 178 µM at 179.85 mbsf, consistent with the influence of the dissolution and/or recrystallization of calcium carbonate in the more calcium carbonate-rich lithostratigraphic Subunit IB.

Calcium concentrations decrease to around 2.4 mM from 28.75 to 47.75 mbsf, then increase with increasing depth to 5.3 mM in the deepest sample at 179.85 mbsf (Fig. 12). Magnesium concentrations generally decrease throughout the section from 51.0 mM at 4.45 mbsf to 32.2 mM at 179.85 mbsf, with a suggestion of slightly higher values from 28.75 to 38.19 mbsf, corresponding to the middle of the depth zone of maximum alkalinity. The decrease in dissolved calcium in the upper sediment indicates that authigenic mineral precipitation is significant in influencing the Ca profile in this depth range, while the magnesium profile appears dominated by the diffusive in-

Table 6. Distribution and abundances of diatoms in Holes 1017A and 1017B.

Core, section, interval	Depth (mbsf)	Abundance	Preservation	<i>Actinocyclus ehrenbergii</i>	<i>Actinocyclus ingens</i>	<i>Actinocyclus oculatus</i>	<i>Actinopychus senarius</i>	<i>Coccolinodiscus marginatus</i>	<i>Coccolinodiscus radiatus</i>	<i>Denticulopsis hustedii</i>	<i>Denticulopsis hyalina</i>	<i>Denticulopsis lauta</i> s.l.	<i>Diploneis</i> sp.	<i>Grammatophora</i> sp.	<i>Hyalodiscus</i> sp.	<i>Neodenticula</i> sp.	<i>Nitzshia</i> cf. <i>reinholdii</i>	<i>Rhizosolenia barboi</i>	<i>Simonseniella (Rhizosolenia) curvirostris</i>	<i>Stephanopyxis turris</i>	<i>Thalassionema nitzschoides</i>	<i>Thalassiosira antiqua</i>	<i>Thalassiosira</i> spp.	Diatom fragments (bands)	Diatom fragments	Sponge spicules		
167-1017A-1H-CC	9.8	T	P																F			F				F		
167-1017B-1H-CC	5.3	B	P																								F	
2H-CC	14.8	T	P																		T			C			F	
3H-CC	24.3	T	P					T								T											R	
4H-CC	33.8	T	P																									C
5H-CC	43.3	T	P	T												T												
6H-CC	52.8	R	P					T	T	T								T									F	
7H-CC	62.3	R	P					F	T	T																	C	
8H-CC	71.8	T	P							T					T												R	
9H-CC	81.3	T	P								T										T						C	
10H-CC	90.8	T	P																					T	T		F	
11H-CC	100.3	T	P	T	T		T							T				T		T							C	
12H-CC	109.8	T	P																T								C	
13H-CC	119.1	T	P																									C
15X-CC	127.3	T	P					T												T								
16X-CC	136.8	T	P					T																			T	
17X-CC	146.5	T	P					T																				C
18X-CC	156.1	T	P																		T							T
19X-CC	165.8	T	P					T																				T
20X-CC	175.4	T	P					T																				C
21X-CC	185.0	T	P		T																							T
22X-CC	194.6	R	P		T			F	T	T							T			F							C	
23X-CC	204.2	B																										F

Note: See “Explanatory Notes” chapter for abbreviations.

fluence of reactions in underlying basalt. Lithium concentrations decrease slightly with depth in the upper sediments, then increase with greater depth to 176 μM at 179.85 mbsf (Fig. 12).

ORGANIC GEOCHEMISTRY

We conducted measurements of elemental composition, volatile hydrocarbons, and heavy hydrocarbons from sediments at Site 1017 (for methods see “Organic Geochemistry” section, “Explanatory Notes” chapter, this volume).

Volatile Hydrocarbons

Because of shipboard safety and pollution prevention considerations, the concentrations of methane, ethane, and propane were routinely monitored at Holes 1017A and 1017B. The results are displayed in Figure 13 and Table 11. Headspace methane concentration increases to 78,000 ppm within the uppermost 20 mbsf. Below 20 mbsf, the concentration varies between 6,000 and 190,000 ppm. Ethane reached its highest level (up to 13 ppm) in the lowermost part of the sequence. Methane/ethane ratios in headspace gas samples show a gradual decrease to values of ~1,500 from top to bottom of the hole (Fig. 15 in the “Site 1014” chapter, this volume), which indicates the addition of thermogenic gas to predominant biogenic gas with increasing depth. No indications for migrated gas could be found. The first obvious gas voids occurred at ~40 mbsf and vacutainer samples were taken whenever voids were observed on the catwalk. Because of the direct gas sampling method, the values of the vacutainer samples are higher but show the same pattern as the headspace samples.

Elemental Analysis

At Site 1017, 72 sediment samples were analyzed for total carbon, inorganic carbon, total nitrogen, and total sulfur (Table 12; Fig. 14).

The percentage of calcium carbonate (CaCO₃) was calculated from the inorganic carbon concentrations by assuming that all carbonate occurs in the form of calcite. CaCO₃ contents vary between ~1 and 22 wt%. The uppermost 120 mbsf are characterized by 10- to 15-m scale cyclic changes in carbonate content. Below 125 mbsf, the amplitude of the fluctuation increases from 5–8 wt% to about 10–15 wt%.

The organic carbon record is characterized by moderately high concentrations between 0.7 and 3.5 wt% throughout the sequence (Table 12; Fig. 14B). Typical total organic carbon (TOC) contents vary between ~1 and 2 wt% until reading 2–3.5 wt% between 170 and 200 mbsf. The organic carbon fluctuation shows no correlation with the cyclic changes in the upper part of the carbonate record (Fig. 14). In the lower part, the increased TOC might be caused by enhanced productivity because low TOC/TN ratios with an average value of ~10 and little fluctuation do not suggest any extra input of terrigenous organic matter (Bordovskiy, 1965; Emerson and Hedges, 1988).

Bitumen Analysis

Long-chain alkenones were analyzed for 30 sediment samples younger than 270 ka in order to estimate paleo-sea-surface temperature (SST). As is shown in Figure 15, alkenones are a major component of extracted lipids. C_{37:2} and C_{37:3} alkenones were identified

Table 7. Distribution and relative abundances of radiolarians in Holes 1017A and 1017B.

Zone	Core, section, interval	Depth (mbsf)	Abundance	Preservation	Actinomma popofskii	Boryostrobos aquilonaris	Boryostrobos praetumidulus	Boryostrobos tumidulus	Ceratospyris hyperborea	Clathrocyclas bicornis	Cycladophora bicincta	Cycladophora davisiana davisiana	Dityophimus cristae	Eucyrtidium calvertense	Eucyrtidium matuyamai	Eucyrtidium tuescheri	Lamprocyrtis heteroporos	Lamprocyrtis neoheteroporos	Lamprocyrtis nigrinatae	Lychnocanoma nipponica sakai	Pterocanium auritum	Pterocanium korotnevi	Pterocorys clausus	Rhizosphaera antarctica	Sphaeropylle langii	Spongostochus glacialis	Stichocorys delmontensis	Stylacanthium acquilionum	Stylatractus universus		
B. aquilonaris	1017A-1H-CC	9.8	R	M						P	P	P	P	P					P	P	P	P	P								
	1017B-1H-CC	5.3	B																												
	2H-CC	14.8	R	G		P			P											P		P	P	P	P	P	P				
	3H-CC	24.3	B																												
	4H-CC	33.8	F	G		P					P	P			P				P	P	P	P		P							
	5H-CC	43.3	R	M		P					P	P								P		P		P							
	6H-CC	52.8	F	G		P		P			P	P		P			P			P		P		P							
	7H-CC	62.3	R	G		P					P	P		P						P		P		P							
	8H-CC	71.8	R	M		P					P	P								P		P		P							
	9H-CC	81.3	B																												
S. universus	10H-CC	90.8	R	G		P					P	P							P		P									P	
	11H-CC	100.3	R	P																P		P								P	
	12H-CC	109.8	R	M		P						P													P					P	
	13H-CC	119.1	B																												
	15X-CC	127.3	R	P																										P	
	16X-CC	136.8	R	P		P	P																								
	17X-CC	146.5	B																												
	18X-CC	156.1	B																												
	19X-CC	165.8	R	M			P					P																		P	
	E. matuyamai	20X-CC	175.4	R	M											P															P
21X-CC		185.0	R	M			P								P															P	
22X-CC		194.6	F	G			P								P															P	
23X-CC		204.2	B																												

Notes: P = present; more detailed abundance information not available. See "Explanatory Notes" chapter for other abbreviations.

based on a comparison of their retention sequences with those in the literature (e.g., ten Haven and Kroon, 1991). Although one peak that eluted earlier than $C_{37:3}$ alkenone seems to be the $C_{37:4}$ alkenone, unequivocal identification was impossible to make in the shipboard laboratory.

The abundances of $C_{37:2}$ and $C_{37:3}$ alkenones, $U_{37}^{k'}$ values, calculated SSTs and carbonate, total organic carbon, total nitrogen, and total sulfur contents are shown in Table 13. The calculation of SST was conducted according to the equation $U_{37}^{k'} = 0.034SST + 0.039$, based on laboratory results for cultured *Emiliania huxleyi* (Prahl et al., 1988) with an estimated analytical accuracy of 0.5% (Prahl and Wakeham, 1987). A shipboard observation of nannofossils in core-catcher (CC) samples showed the presence of *Gephyrocapsa oceanica* as well as *E. huxleyi* (see "Biostratigraphy" section, this chapter), both of which produce long-chain alkenones (Marlowe et al., 1990). *G. oceanica* shows a different $U_{37}^{k'}$ temperature relationship from that of *E. huxleyi* (Volkman et al., 1995). Thus, the recalculation of SST is necessary based on paleontological and further geochemical data for the relative abundances of *E. huxleyi* and *G. oceanica* from shore-based studies. Nevertheless, as is shown in Figure 16, the calculated SST shows a significant variation between 10.4° and 18.0°C .

Although the number of samples is limited, a correlation exists between C_{37} alkenone abundance and $U_{37}^{k'}$, and between total organic carbon content and $U_{37}^{k'}$ (Fig. 17). Both C_{37} alkenone abundance and TOC content show higher concentrations with warmer estimated temperatures (Fig. 16). Since long-chain alkenones were biosynthesized exclusively by some Prymnesiophyte algae, (e.g., *E. huxleyi* and some species of genus *Gephyrocapsa*) and survived digestion and bacterial degradation (Brassell, 1993), a positive correlation between C_{37} alkenone abundances and $U_{37}^{k'}$ (Fig. 17) indicates that productivity of nannoplanktons was higher in warmer periods than in cooler periods. The higher TOC content in warmer periods might, therefore, directly reflect high productivity of nannoplanktons.

PHYSICAL PROPERTIES

Multisensor Track Measurements

The shipboard physical properties program at Site 1017 included nondestructive measurements of bulk density, magnetic susceptibility, P -wave velocity, and natural gamma-ray activity on whole sections of all cores using the MST (Fig. 18). Magnetic susceptibility was measured at 4-cm intervals at low sensitivity (1-s measuring time) on all Site 1017 cores. GRAPE bulk density measurements were made at 4-cm intervals on all Site 1017 cores. PWL velocity measurements were made at 4-cm intervals on the first four cores from Holes 1017A, 1017B, and 1017C. Below the fourth core in each hole the PWL gave poor results because of signal attenuation and sediment cracking resulting from high gas content (see "Organic Geochemistry" section, this chapter) and was therefore deactivated. Natural gamma-ray activity was measured with a 15-s count every 12 cm on cores from Holes 1017A, 1017B, and 1017C and not measured on cores from Holes 1017D and 1017E.

Index Properties

Index properties measurements were made at one sample per working section in all cores from Hole 1017B. Index properties of bulk density, void ratio, porosity, water content, dry-bulk density, and grain density were determined by the gravimetric Method C (see "Physical Properties" section, "Explanatory Notes" chapter, this volume) and are shown in Figure 19 (Table 14 on CD-ROM in the back pocket of this volume). Figure 20 shows bulk density with the GRAPE density record smoothed with a 70-point running average to dampen the higher frequencies. The observed correlation gives us confidence that the subtle variations in values of index properties downhole, perhaps seen as scatter, do not necessarily result from a

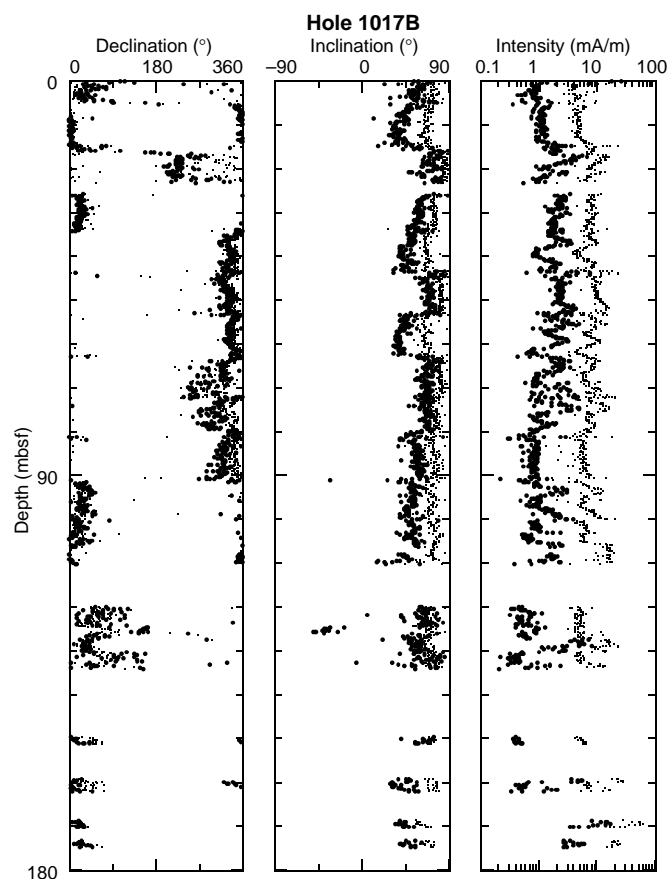


Figure 7. Plots of magnetic declination, inclination, and intensity of APC (0–109.8 mbsf) and XCB cores from Hole 1017B. Small and large dots represent the data before and after AF demagnetization at 15 mT, respectively.

range of error in the measurements. Rather, they reflect the fluctuating levels of nannofossils (see “Lithostratigraphy” section, this chapter), which have been shown to correlate well with variations in density (see “Physical Properties” sections, “Site 1010” and “Site 1011” chapters, this volume).

Compressional-Wave Velocity

Because of the gassy nature of the sediments (see “Organic Geochemistry” section, this chapter) velocity could be measured only through Section 167-1017B-2H-4. The three measured values were higher than at other sites on this leg, ranging from 1586 to 1607 m/s to depths of only 10 mbsf.

Heat Flow

Thermal conductivity was measured to 80.05 mbsf in Hole 1017B (Table 15 on CD-ROM in the back pocket of this volume). Three downhole temperature measurements were taken with the APC Adara temperature tool in Hole 1017B: 6.5°C at 33.8 mbsf, 7.8°C at 52.8 mbsf, and 9.3°C at 71.8 mbsf in Cores 167-1017B-4H, 6H, and 8H, respectively (Fig. 21). Bottom-water temperature was measured on all runs indicating a bottom-water temperature of 4.0°C ± 0.1°C. The four data points yield a thermal gradient of 74°C/km (Fig. 22). Using an average measured thermal conductivity of 0.937 W/(m·K) provides a heat-flow estimate of 70 mW/m² at Site 1017.

Color Reflectance

Color reflectance was measured at 4- to 6-cm intervals on all Site 1017 cores. Reflectance is generally low, averaging about 10% for the 450–500-nm band, and variations are subtle, ranging from 5% to 13%. This is primarily because of the dominant clays and silts throughout the Site 1017 stratigraphy (see “Lithostratigraphy” section, this chapter). Despite the uniform character of the sediments, both Holes 1017B and 1017C show orbital-scale variability in the color reflectance data (Fig. 23). Based on the age-depth control points for Site 1017 (see “Composite Depths and Sedimentation Rates” section, this chapter), 45 mbsf is equivalent to roughly 270 ka. Also plotted in Figure 23A are the preliminary estimates of sea-surface temperature (SST) for 0–45 mbsf of Hole 1017B based on the alkenone unsaturation index (see “Organic Geochemistry” section, this chapter). Intervals of higher reflectance correspond to intervals with lower estimated SSTs, suggesting that glacial intervals are marked by cooler temperatures and higher color reflectance values. This is not true for the interval from ~20 to 30 mbsf.

Digital Color Video

All cores from Holes 1017B, 1017C, and 1017D were imaged with the ODP color digital imaging system over 20-cm intervals, providing a 0.25-mm pixel. Video images from Holes 1017B, 1017C, and 1017D show hole-to-hole correlation of intensity of color CIELAB L* (Fig. 24).

SUMMARY

Drilling at Site 1017, which is the seaward site of the Conception Transect, was planned to collect a high-resolution upper Pliocene to Holocene sediment column. We underestimated sedimentation rates prior to drilling, and instead recovered sediments from about 0 to 1.4 Ma in the 204-m-thick drilled sediment section (Fig. 25). Sedimentation rates near 200 m/m.y. should make this an important upper Pleistocene, high-resolution section. Because correlations were difficult using the MST data, no continuous section was identified by the shipboard party. Five holes were drilled to 9.8 mbsf, four were drilled to 25 mbsf, and three holes covered the upper 108 mbsf (~0.7 Ma). Although the site was double-cored to 174 mbsf (~1.1 Ma), loss of sediment cores on both deep holes caused large coring gaps, especially around 115 mbsf. The Quaternary sediment section at Site 1017 consists of hemipelagic silts and clays interbedded with frequent thin turbidites, becoming slightly more nannofossil enriched below 74 mbsf (~0.4–1.4 Ma). Foraminifers, diatoms, and radiolarians are also present in the sediment column.

REFERENCES

- Bordovskiy, O.K., 1965. Accumulation and transformation of organic substances in marine sediment, 2. Sources of organic matter in marine basins. *Mar. Geol.*, 3:5–31.
- Brassell, S.C., 1993. Applications of biomarkers for delineating marine paleoclimatic fluctuations during the Pleistocene. In Engel, M.H., and Macko, S.A. (Eds.), *Organic Geochemistry: Principles and Applications*: New York (Plenum), 699–738.
- Emerson, S., and Hedges, J.L., 1988. Processes controlling the organic carbon content of open ocean sediments. *Paleoceanography*, 3:621–634.
- Jones, B.H., Brink, K.H., Dugdale, R.C., Stuart, D.W., van Leer, J.C., Blasco, D., and Kelley, J.C., 1983. Observations of a persistent upwelling center off Point Conception, California. In Suess, E., and Thiede, J. (Eds.), *Coastal Upwelling: Its Sediment Record*: New York (Plenum), 37–60.

- Lyle, M., Gallaway, P.J., Liberty, L.M., Mix, A., Stott, L., Hammond, D., Gardner, J., Dean, W., and the EW9504 Scientific Party, 1995a. Data submission. W9406 and EW9504 site surveys of the California margin proposed drillsites, Leg 167 (Vol. 1): Site maps and descriptions. Boise State Univ., *CGISS Tech. Rep.*, 95-11.
- , 1995b. Data submission. W9406 and EW9504 site surveys of the California margin proposed drillsites, Leg 167 (Vol. 2): Seismic profiles. Boise State Univ., *CGISS Tech. Rep.*, 95-12.
- Marlowe, I.T., Brassell, S.C., Eglinton, G., and Green, J.C., 1990. Long-chain alkenones and alkyl alkenoates and the fossil coccolith record of marine sediments. *Chem. Geol.*, 88:349-375.
- Middelburg, J.J., de Lange, G.J., and Kreulen, R., 1990. Dolomite formation in anoxic sediments of Kau Bay, Indonesia. *Geology*, 18:399-402.
- Pisias, N.G., Mayer, L.A., Janecek, T.R., Palmer-Julson, A., and van Andel, T.H. (Eds.), 1995. *Proc. ODP, Sci. Results*, 138: College Station, TX (Ocean Drilling Program).
- Prahl, F.G., Muehlhausen, L.A., and Zahnle, D.L., 1988. Further evaluation of long-chain alkenones as indicators of paleoceanographic conditions. *Geochim. Cosmochim. Acta*, 52:2303-2310.
- Prahl, F.G., and Wakeham, S.G., 1987. Calibration of unsaturation patterns in long-chain ketone compositions for paleotemperature assessment. *Nature*, 330:367-369.
- Sorlien, C., 1994. Structure and Neogene evolution of offshore Santa Maria Basin and Western Santa Barbara Channel, California. [Ph.D. dissert.]. Univ. of California, Santa Barbara.
- ten Haven, H.L., and Kroon, D., 1991. Late Pleistocene sea surface water temperature variations off Oman as revealed by the distribution of long-chain alkenones. In Prell, W.L., Niituma, N., et al., *Proc. ODP, Sci. Results*, 117: College Station, TX (Ocean Drilling Program), 445-452.
- Volkman, J.K., Barrett, S.M., Blackburn, S.I., and Sikes, E.L., 1995. Alkenones in *Gephyrocapsa oceanica*: implications for studies of paleoclimate. *Geochim. Cosmochim. Acta*, 59:513-520.

Ms 167-111

NOTE: For all sites drilled, core-description forms (“barrel sheets”) and core photographs can be found in Section 3, beginning on page 499. Smear-slide data can be found in Section 4, beginning on page 1327. See Table of Contents for material contained on CD-ROM.

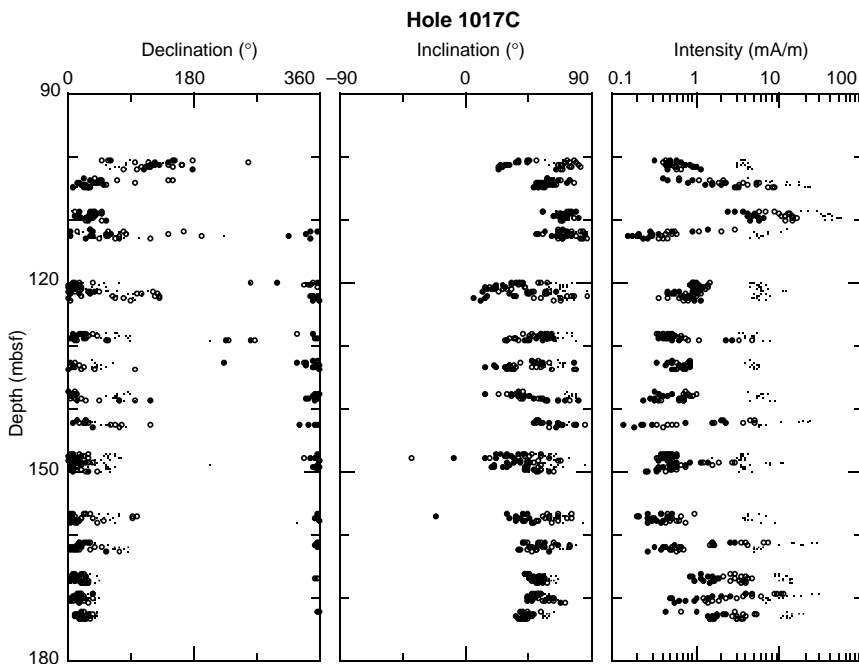


Figure 8. Plots of magnetic declination, inclination, and intensity of selected sections from XCB cores of Hole 1017C. Small dots represent the NRM data. Open and closed circles represent magnetization after AF treatment at 15 mT and 25 mT, respectively.

Table 8. Site 1017 composite depth section.

Core, section	Depth (mbsf)	Offset (m)	Depth (mcd)
167-1017A-1H-1	0.00	1.42	1.42
167-1017B-			
1H-1	0.00	0.30	0.30
2H-1	5.30	0.70	6.00
3H-1	14.80	5.42	20.22
4H-1	24.30	3.19	27.49
5H-1	33.80	3.89	37.69
6H-1	43.30	5.64	48.94
7H-1	52.80	7.49	60.29
8H-1	62.30	8.68	70.98
9H-1	71.80	12.00	83.80
10H-1	81.30	12.00	93.30
11H-1	90.80	12.00	102.80
12H-1	100.30	13.66	113.96
15X-1	119.30	17.84	137.14
16X-1	127.30	18.97	146.27
17X-2	137.53	18.97	156.50
18X-2	146.74	19.18	165.92
19X-1	156.10	19.18	175.28
20X-1	165.80	19.15	184.95
21X-1	175.40	16.92	192.32
22X-1	185.00	16.92	201.92
23X-1	194.60	16.92	211.52
167-1017C-			
1H-1	0.00	0.00	0.00
2H-1	7.30	1.70	9.00
3H-1	16.80	4.61	21.41
4H-1	26.30	5.31	31.61
5H-1	35.80	5.48	41.28
6H-1	45.30	7.50	52.80
7H-1	54.80	8.38	63.18
8H-1	64.30	11.26	75.56
9X-1	73.80	12.48	86.28
10X-1	78.30	14.02	92.32
11X-1	87.90	14.97	102.87
12X-1	97.50	14.97	112.47
13X-1	107.10	15.69	122.79
14X-1	116.80	15.69	132.49
15X-1	126.40	15.69	142.09
16X-1	135.90	18.62	154.52
17X-1	145.50	18.28	163.78
18X-1	155.10	18.27	173.37
19X-1	164.70	19.59	184.29
167-1017D-			
1H-1	0.00	0.00	0.00
2H-1	4.10	3.42	7.52
3H-1	13.60	4.08	17.68
4H-1	23.10	4.04	27.14
5H-1	32.60	5.46	38.06
6H-1	42.10	6.55	48.65
7H-1	51.60	8.57	60.17
8H-1	61.10	8.44	69.54
9H-1	70.60	12.09	82.69
167-1017E-			
1H-1	0.00	0.00	0.00
2H-1	5.90	3.30	9.20
3H-1	15.40	4.47	19.87

Note: This table is also on CD-ROM, back pocket, this volume.

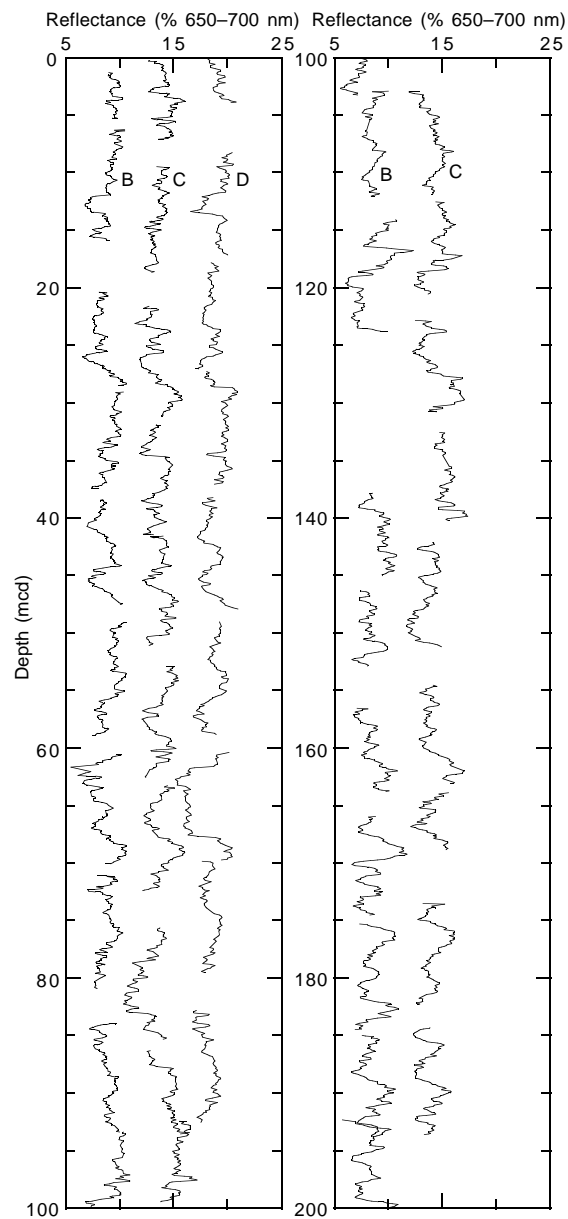


Figure 9. Smoothed (20-cm Gaussian) color reflectance (% 650–700 nm band) data for the upper 200 m from Site 1017 on the mcd scale. Holes 1017B, 1017C, and 1017D are offset from each other by a constant (5%).

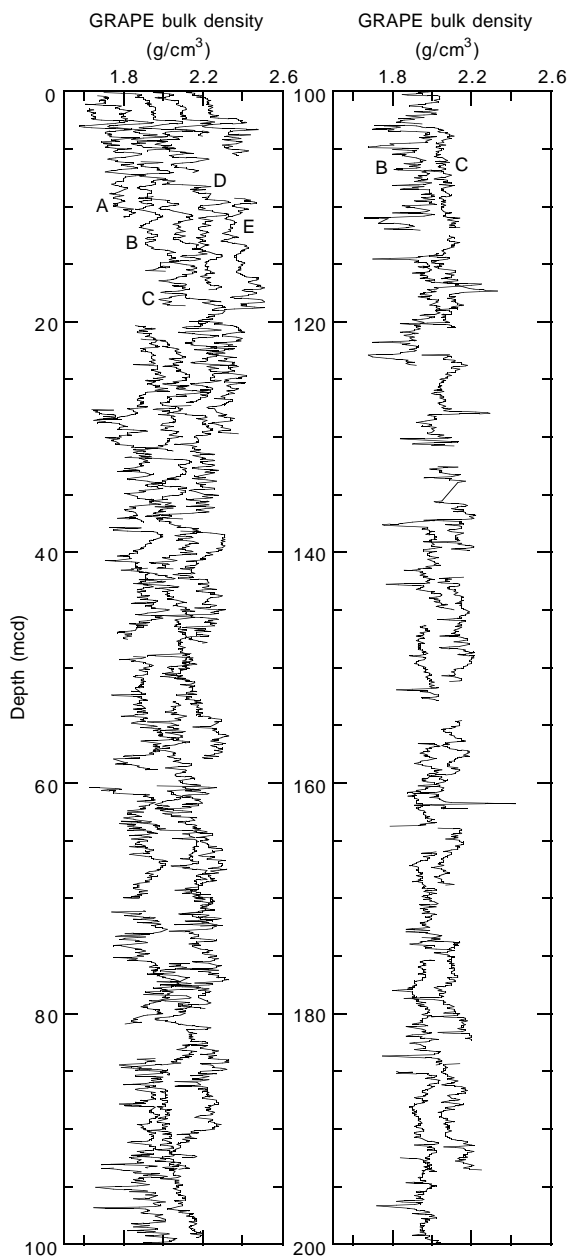


Figure 10. Smoothed (15-cm Gaussian) GRAPE bulk density data for the upper 200 m from Site 1017 on the mcd scale. Holes 1017A, 1017B, 1017C, 1017D, and 1017E are offset from each other by a constant (0.15 g/cm³).

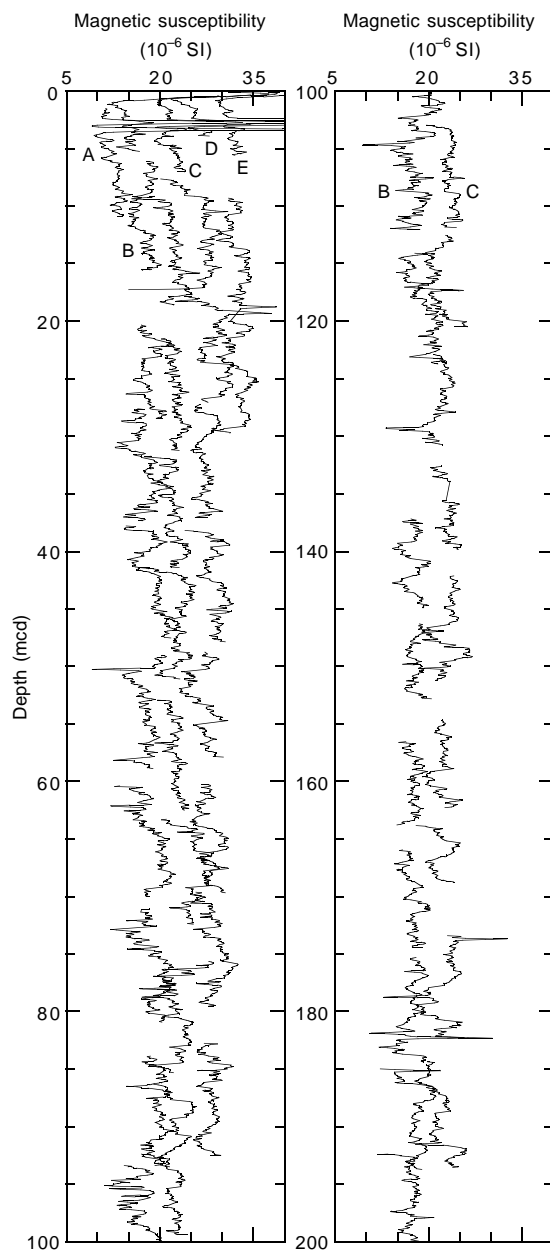


Figure 11. Smoothed (15-cm Gaussian) magnetic susceptibility data for the upper 150 m from Site 1017 on the mcd scale. Holes 1017A, 1017B, 1017C, 1017D, and 1017E are vertically offset from each other by a constant (5×10^{-6} SI).

Table 9. Site 1017 sedimentation rates.

Event	Depth (mcd)	Age (Ma)	Sedimentation rate (mcd/m.y.)
	0	0	
Acme <i>E. huxley</i>	10.750	0.085	126.47
<i>T. P. lacunosa</i>	97.435	0.460	231.16
T large <i>Gephyrocapsa</i> spp.	189.090	1.240	117.51

Note: T = top.

Table 10. Interstitial water geochemical data, Site 1017.

Core, section, interval (cm)	Depth (mbsf)	pH	Alkalinity (mM)	Salinity	Cl ⁻ (mM)	Na ⁺ (mM)	SO ₄ ²⁻ (mM)	HPO ₄ ²⁻ (μM)	NH ₄ ⁺ (mM)	H ₄ SiO ₄ (mM)	Ca ²⁺ (mM)	Mg ²⁺ (mM)	Sr ²⁺ (μM)	Li ⁺ (μM)	K ⁺ (mM)
167-1017B-1H-3, 145-150	4.45	7.68	3.68	34.0	549	478	29.0	10	0.15	522	10.2	51.0	88	26	10.5
167-1017A-1H-4, 145-150	5.67	7.58	11.3	34.0	551		23.9	49	0.99	635	8.92	51.2	86	22	ND
167-1017B-2H-3, 145-150	9.75	8.02	24.1	34.0	553	481	11.7	110	2.18	762	6.26	48.6	87	21	10.2
3H-3, 145-150	19.25	7.61	43.7	34.0	549	481	<1.4	161	4.82	779	2.88	47.5	88	26	10.4
4H-3, 145-150	28.75	7.70	44.6	34.0	552	483	<1.4	93	5.14	786	2.37	48.9	87	30	10.7
5H-3, 145-150	38.19	7.60	44.1	34.0	556	487	<1.4	117	5.92	796	2.48	48.4	83	31	11.0
6H-3, 145-150	47.75	7.60	41.8	33.0	552	485	<1.4	115	6.26	902	2.35	46.7	83	35	10.7
9H-3, 145-150	76.25	7.66	35.3	32.5	548	488	<1.4	59	8.32	953	3.29	39.2	103	59	10.6
12H-3, 145-150	104.75	7.19	31.3	36.0	545	491	<1.4	40	8.14	1015	4.02	33.5	115	84	10.6
15X-3, 145-150	122.88	7.48	35.7	33.0	547	493	<1.4	42	8.79	910	3.92	35.8	122	91	10.6
18X-3, 145-150	149.69	7.18	32.5	36.0	546	494	<1.4	22	8.64	1005	4.15	32.8	142	137	10.4
21X-3, 145-150	179.85	7.22	33.1	32.0	545	493	<1.4	12	8.53	917	5.34	32.2	178	176	10.2

Note: ND = value not determined.

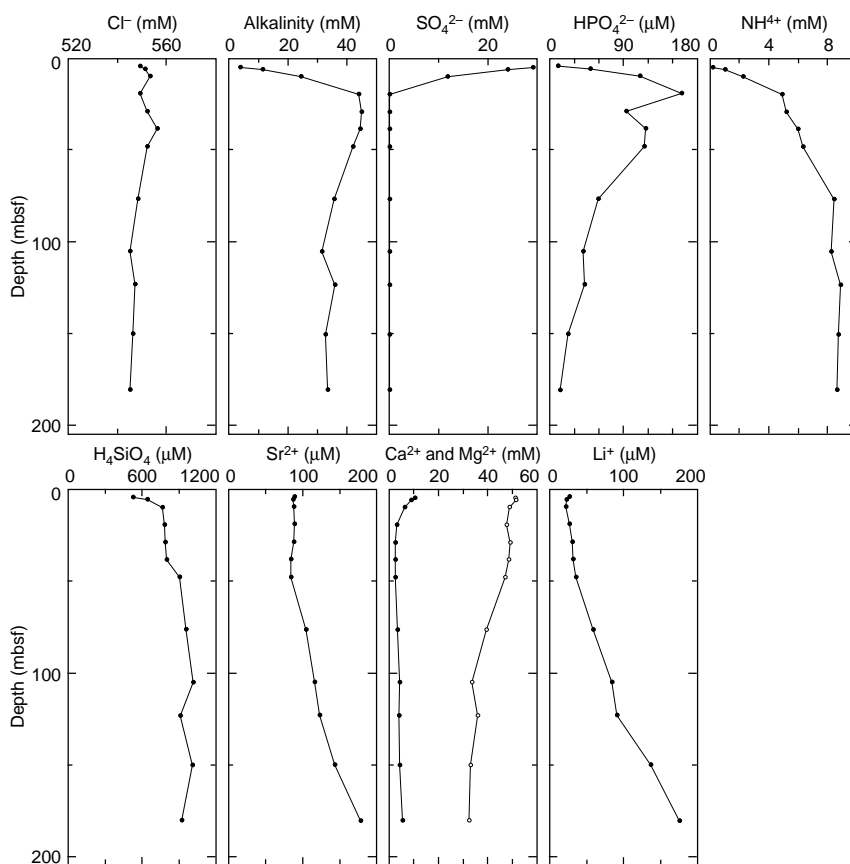


Figure 12. Interstitial water geochemical data, Site 1017. Solid circles = Ca, open circles = Mg.

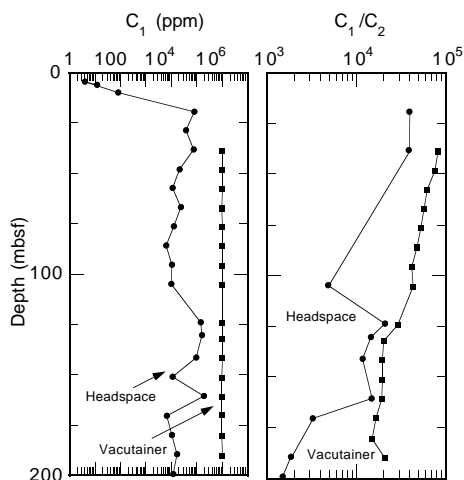


Figure 13. Depth variations of methane concentration (C_1) and methane/ethane (C_1/C_2) ratio in Holes 1017A and 1017B.

Table 11. Concentrations of methane (C_1), ethane (C_2), propane (C_3), and methane/ethane ratio (C_1/C_2) obtained by the headspace and vacutainer techniques from Holes 1017A and 1017B.

Core, section, interval (cm)	Depth (mbsf)	C_1 (ppm)	C_2 (ppm)	C_3 (ppm)	C_1/C_2
Headspace					
167-1017A-1H-5, 0-5	6.03	12			
167-1017B-					
1H-4, 0-5	4.53	4			
2H-4, 0-5	9.83	82			
3H-4, 0-5	19.33	78,586	2		39,293
4H-4, 0-5	28.83	37,857			
5H-4, 0-5	38.33	76,529	2		38,265
6H-4, 0-5	47.83	20,965			
7H-4, 0-5	57.33	11,322			
8H-4, 0-5	66.83	23,667			
9H-4, 0-5	76.33	12,614			
10H-4, 0-5	85.83	6,144			
11H-4, 0-5	95.33	10,301			
12H-4, 0-5	104.83	9,663	2		4,832
15X-4, 0-5	123.83	145,758	7	3	20,823
16X-3, 0-5	130.33	160,562	11	5	14,597
17X-4, 0-5	141.33	94,254	8	6	11,782
18X-4, 0-5	151.03	11,314			
19X-4, 0-5	160.63	192,520	13	6	14,809
20X-4, 0-5	170.33	6,478	2	1	3,239
21X-4, 0-5	179.93	10,818			
22X-4, 0-5	189.53	16,470	9	7	1,830
23X-2, 0-5	196.13	11,944	8	5	1,493
Vacutainer					
167-1017B-					
5H-4, 50-51	38.81	985,687	12	5	82,141
6H-4, 50-51	48.31	992,992	13	4	76,384
7H-4, 50-51	57.81	989,967	16	5	61,873
8H-4, 50-51	67.31	970,208	17	5	57,071
9H-4, 50-51	76.81	999,999	19	5	52,632
10H-4, 50-51	86.31	995,087	21	5	47,385
11H-4, 50-51	95.81	1,002,520	24	7	41,772
12H-4, 50-51	105.31	1,002,520	23	7	43,588
15X-4, 50-51	124.31	992,393	34	9	29,188
16X-4, 50-51	132.31	978,072	48	13	20,377
17X-4, 50-51	141.81	987,918	50	14	19,758
18X-4, 50-51	151.51	967,777	49	14	19,751
19X-4, 50-51	161.11	973,511	51	14	19,088
20X-4, 50-51	170.11	940,755	57	17	16,504
21X-4, 50-51	180.41	932,415	62	17	15,039
22X-4, 50-51	190.01	1,005,620	48	11	20,950

Table 12. Concentrations of inorganic carbon, calcium carbonate, total carbon, total organic carbon, total nitrogen, and total sulfur in weight percent (wt%) in Hole 1017B.

Core, section, interval (cm)	Depth (mbsf)	Inorganic carbon (wt%)	CaCO ₃ (wt%)	Total carbon (wt%)	Total organic carbon (wt%)	Total nitrogen (wt%)	Total sulfur (wt%)	Total organic carbon/total nitrogen
167-1017B-								
1H-1, 28-29	0.28	0.97	8.1	3.45	2.48	0.29	0.42	8.6
1H-3, 29-30	3.29	1.03	8.6	2.4	1.37	0.14	0.36	9.8
2H-1, 29-30	5.59	1.16	9.7	2.4	1.24	0.11	0.67	11.3
2H-3, 29-30	8.59	0.8	6.7	2.27	1.47	0.15	0.71	9.8
2H-5, 29-30	11.59	0.84	7	2.57	1.73	0.18	0.66	9.6
2H-7, 29-30	14.59	0.57	4.7	1.49	0.92	0.11	0.57	8.4
3H-2, 29-30	16.59	0.31	2.6	1.83	1.52	0.16	0.58	9.5
3H-4, 29-30	19.59	0.55	4.6	1.65	1.1	0.13	0.61	8.5
3H-6, 29-30	22.59	1.36	11.3	2.99	1.63	0.19	0.65	8.6
4H-2, 28-29	26.08	0.96	8	2.07	1.11	0.12	0.85	9.3
4H-4, 29-30	29.09	0.93	7.7	2.09	1.16	0.11	0.75	10.5
4H-6, 29-30	32.2	0.77	6.4	1.79	1.02	0.09	0.64	11.3
5H-1, 68-69	34.48	0.53	4.4	1.81	1.28	0.13	0.75	9.8
5H-3, 29-30	37.03	0.64	5.3	3.09	2.45	0.24	0.83	10.2
5H-5, 29-30	40.03	0.85	7.1	2.12	1.27	0.12	0.6	10.6
5H-7, 29-30	43.1	1.1	9.2	2.82	1.72	0.19	0.94	9.1
6H-2, 28-29	45.08	1.41	11.7	2.79	1.38	0.14	0.91	9.9
6H-4, 28-29	48.08	1.5	12.5	2.78	1.28	0.14	0.8	9.1
6H-6, 27-28	51.17	0.5	4.2	2.24	1.74	0.16	0.77	10.9
7H-1, 72-73	53.52	0.7	5.8	2.06	1.36	0.15	0.88	9.1
7H-3, 32-33	56.12	0.55	4.6	2.11	1.56	0.17	1.19	9.2
7H-5, 32-33	59.12	0.55	4.6	2.58	2.03	0.19	0.81	10.7
7H-7, 29-30	62.09	1.17	9.7	2.39	1.22	0.12	0.61	10.2
8H-3, 29-30	64.39	1.03	8.6	2.22	1.19	0.13	0.54	9.2
8H-5, 29-30	67.39	0.85	7.1	1.99	1.14	0.14	0.76	8.1
8H-7, 29-30	70.39	0.46	3.8	2.37	1.91	0.19	1.01	10.1
9H-1, 29-30	72.09	0.54	4.5	2.33	1.79	0.18	0.94	9.9
9H-3, 29-30	75.09	0.96	8	3.13	2.17	0.21	0.91	10.3
9H-5, 29-30	78.09	1.24	10.3	3.19	1.95	0.21	1	9.3
9H-7, 29-30	81.09	0.92	7.7	1.98	1.06	0.1	0.71	10.6
10H-2, 29-30	83.09	1.04	8.7	2.02	0.98	0.09	0.53	10.9
10H-4, 29-30	86.01	0.61	5.1	0.99	0.38	0.4	0.45	1
10H-6, 29-30	89.01	0.82	6.8	2.15	1.33	0.14	0.89	9.5
11H-1, 85-86	91.65	0.65	5.4	1.98	1.33	0.15	0.93	8.9
11H-3, 29-30	94.03	0.97	8.1	2.95	1.98	0.18	0.85	11
11H-5, 29-30	97.03	1.22	10.2	2.89	1.67	0.16	0.92	10.4
11H-7, 29-30	100.03	1.10	9.2	2.93	1.83	0.18	1.06	10.2
12H-2, 29-30	102.09	1.39	11.6	3.13	1.74	0.16	1.35	10.9
12H-4, 29-30	105.09	1.12	9.3	2.61	1.49	0.15	1.05	9.9
1017C-13X-1, 29-30	107.39	0.60	5	2.65	2.05	0.19	0.65	10.8
1017B-12H-6, 28-29	108.11	1.02	8.5	3.43	2.41	0.21	1.05	11.5
1017C-13X-3, 29-30	110.39	0.72	6	3.48	2.76	0.26	1.08	10.6
1017C-13X-5, 29-30	113.39	1.07	8.9	2.82	1.75	0.19	0.84	9.2
1017C-14X-1, 29-30	117.09	0.80	6.7	1.46	0.66	0.08	0.36	8.3
1017B-15X-1, 28-29	119.58	0.94	7.8	2.22	1.28	0.11	0.6	11.6
1017C-14X-3, 29-30	120.09	1.30	10.8	2.5	1.2	0.14	0.83	8.6
1017B-15X-3, 28-29	121.71	1.07	8.9	2.03	0.96	0.12	0.58	8
1017C-14X-5, 27-28	123.07	1.59	13.2	2.79	1.2	0.15	0.43	8
1017B-15X-5, 28-29	124.71	1.59	13.2	2.82	1.23	0.13	0.67	9.5
167-1017B-								
16X-1, 28-29	127.58	1.02	8.5	2.57	1.55	0.18	0.77	8.6
16X-3, 29-30	130.59	1.65	13.7	3.85	2.2	0.2	0.55	11
16X-5, 29-30	133.59	0.86	7.2	2.14	1.28	0.12	0.34	10.7
17X-2, 27-28	137.8	1.46	12.2	2.81	1.35	0.13	0.41	10.4
17X-4, 27-28	140.8	1.52	12.7	3.25	1.73	0.17	0.92	10.2
17X-6, 27-28	143.8	1.65	13.7	2.96	1.31	0.16	0.81	8.2
18X-3, 28-29	148.52	1.86	15.5	4.91	3.05	0.24	0.81	12.7
18X-5, 28-29	151.52	1.59	13.2	3.23	1.64	0.15	0.94	10.9
18X-7, 28-29	154.52	0.41	3.4	2.39	1.98	0.19	0.97	10.4
19X-2, 29-30	157.89	1.87	15.6	3.66	1.79	0.19	0.92	9.4
19X-4, 29-30	160.89	1.22	10.2	2.48	1.26	0.11	0.68	11.5
19X-6, 29-30	163.89	2.21	18.4	3.79	1.58	0.13	0.21	12.2
20X-1, 28-29	166.08	2.59	21.6	4.57	1.98	0.21	0.62	9.4
20X-3, 28-29	169.08	1.21	10.1	4.15	2.94	0.26	1.94	11.3
20X-5, 28-29	172.08	2.18	18.2	3.53	1.35	0.13	0.29	10.4
21X-1, 29-30	175.69	0.79	6.6	4.42	3.63	0.28	0.83	13
21X-3, 29-30	178.69	0.67	5.6	3.69	3.02	0.23	0.99	13.1
21X-5, 29-30	181.69	1.44	12	4.69	3.25	0.29	1.19	11.2
21X-7, 29-30	184.11	1.31	10.9	4.1	2.79	0.23	0.99	12.1
22X-2, 29-30	186.79	1.52	12.7	3.86	2.34	0.22	1.96	10.6
22X-4, 29-30	189.79	1.54	12.8	4.75	3.21	0.27	0.9	11.9
22X-6, 29-30	192.79	0.65	5.4	4.26	3.61	0.28	1.46	12.9
23X-1, 89-90	195.49	0.55	4.6	3.27	2.72	0.24	0.11	11.3

Notes: Missing or incomplete core data in Hole 1017B were supplemented by core data from Hole 1017C. This table is also on CD-ROM, back pocket, this volume.

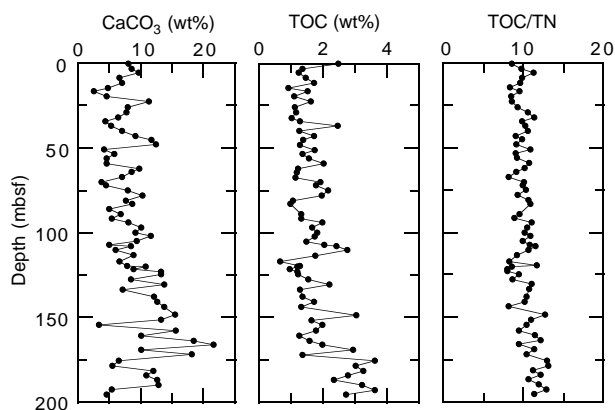


Figure 14. Depth variations of calcium carbonate, total organic carbon (TOC), and total organic carbon/total nitrogen (TOC/TN) in sediments of Hole 1017B.

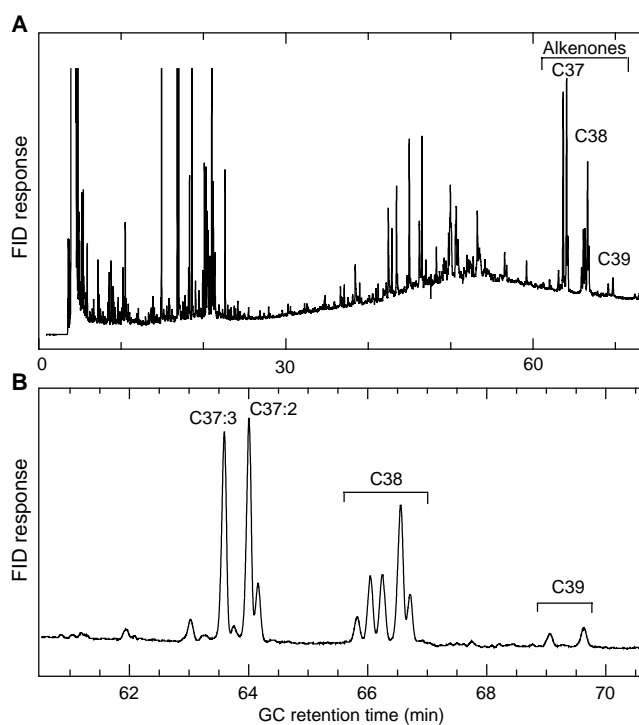


Figure 15. **A.** Gas chromatogram showing C_{37} to C_{39} alkenones of the total extract from Sample 167-1017-5H-6. **B.** Enlarged area of alkenone elution.

Table 13. The abundances of $C_{37:2}$ and $C_{37:3}$ alkenones, U_{37}^k values, calculated SSTs, calcium carbonate, total organic carbon, and total nitrogen contents in selected samples from Hole 1017B.

Core, section, interval (cm)	Depth (mbsf)	U_{37}^k	SST (°C)	$C_{37:3}$ ($\mu\text{g/g-rock}$)	$C_{37:2}$ ($\mu\text{g/g-rock}$)	total C_{37} ($\mu\text{g/g-rock}$)	CaCO_3 (wt%)	TOC (wt%)	TOC/TN
167-1017B-									
1H-1, 65-67	0.65	0.54	14.7	0.61	0.71	1.33	8.42	2.34	8.07
1H-2, 65-67	2.15	0.55	15.0	1.25	1.51	2.76	17.50	1.64	8.63
1H-3, 76-78	3.76	0.54	14.9	0.50	0.60	1.10	10.25	1.42	7.89
2H-1, 65-67	5.95	0.44	11.9	0.24	0.19	0.43	5.75	0.87	7.25
2H-2, 65-67	7.45	0.42	11.2	0.39	0.28	0.67	7.17	1.24	8.86
2H-3, 65-67	8.95	0.50	13.6	0.37	0.37	0.75	7.42	1.40	9.33
2H-4, 65-67	10.45	0.49	13.2	0.14	0.13	0.27	6.75	1.41	9.40
2H-5, 65-67	11.95	0.43	11.6	0.62	0.48	1.09	6.50	1.57	9.81
2H-6, 65-67	13.45	0.43	11.4	0.65	0.49	1.14	8.00	0.84	7.64
2H-7, 50-52	14.8	0.47	12.7	0.89	0.78	1.67	5.25	1.61	8.94
3H-1, 65-67	15.45	0.55	15.1	0.74	0.90	1.64	4.92	1.70	9.44
3H-2, 65-67	16.95	0.55	15.1	0.78	0.96	1.73	3.58	2.07	9.41
3H-3, 65-67	18.45	0.55	15.0	1.89	2.31	4.20	5.42	1.76	9.78
3H-4, 65-67	19.95	0.50	13.5	0.73	0.72	1.45	4.08	1.51	9.44
3H-5, 65-67	21.45	0.65	18.0	0.99	1.85	2.84	7.50	2.23	9.70
3H-6, 65-67	22.95	0.64	17.8	0.68	1.24	1.92	10.33	1.56	9.18
4H-1, 65-67	24.95	0.63	17.3	1.54	2.60	4.14	7.58	1.97	9.85
4H-2, 65-67	26.45	0.55	15.0	0.54	0.66	1.20	8.00	1.32	8.25
4H-3, 65-67	27.95	0.51	13.9	0.68	0.70	1.38	9.75	0.89	6.36
4H-4, 65-67	29.45	0.49	13.4	0.44	0.43	0.87	8.00	0.86	5.38
4H-5, 65-67	31.01	0.42	11.3	0.47	0.34	0.81	7.25	0.94	6.71
4H-6, 65-67	32.56	0.48	12.9	0.29	0.26	0.55	5.25	0.91	9.10
4H-7, 65-67	34.12	0.47	12.7	0.69	0.61	1.31	5.83	1.2	19.31
5H-1, 65-67	34.45	0.53	14.5	0.64	0.73	1.36	4.33	1.17	8.36
5H-2, 65-67	35.89	0.52	14.1	0.39	0.42	0.82	3.33	1.53	8.05
5H-3, 65-67	37.39	0.61	16.9	1.17	1.86	3.03	7.75	2.29	10.90
5H-4, 65-67	38.89	0.42	11.3	0.51	0.37	0.88	6.25	1.36	13.60
5H-5, 65-67	40.39	0.39	10.4	0.50	0.32	0.82	5.08	0.87	8.70
5H-6, 65-67	41.92	0.52	14.2	1.10	1.20	2.30	1.83	2.26	11.30
5H-7, 65-67	43.46	0.60	16.6	0.46	0.71	1.17	10.50	1.72	7.82

Note: SST = sea-surface temperature.

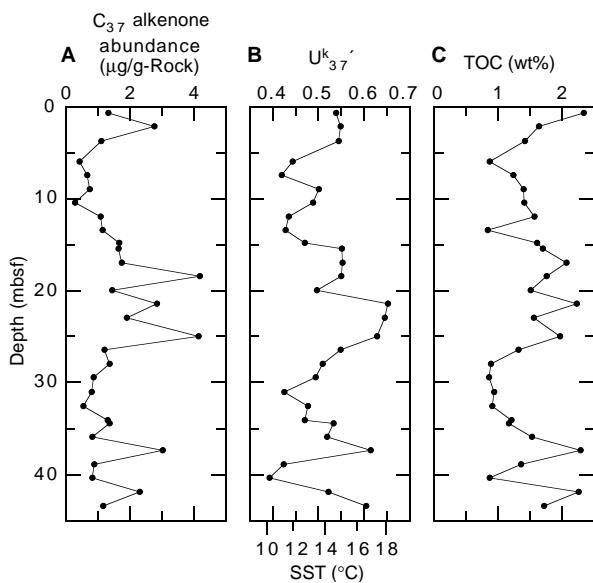


Figure 16. Depth variations of (A) C₃₇ alkenone abundance, (B) U₃₇^{k'} value and calculated SST, and (C) total organic carbon (TOC) contents in sediments of Hole 1017B.

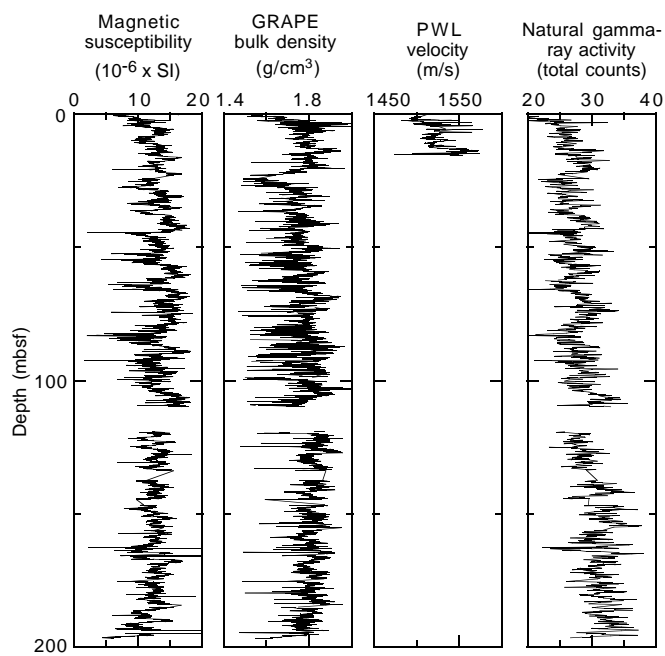


Figure 18. MST data from Hole 1017B.

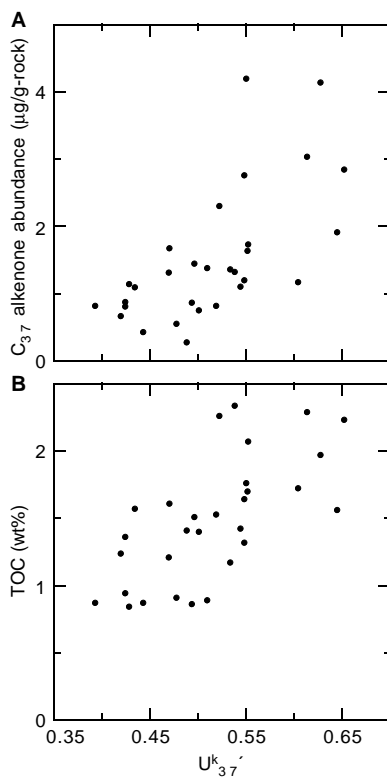


Figure 17. Diagrams of (A) C₃₇ alkenone abundance and (B) total organic carbon content (TOC) vs. U₃₇^{k'} value in sediments of Hole 1017B.

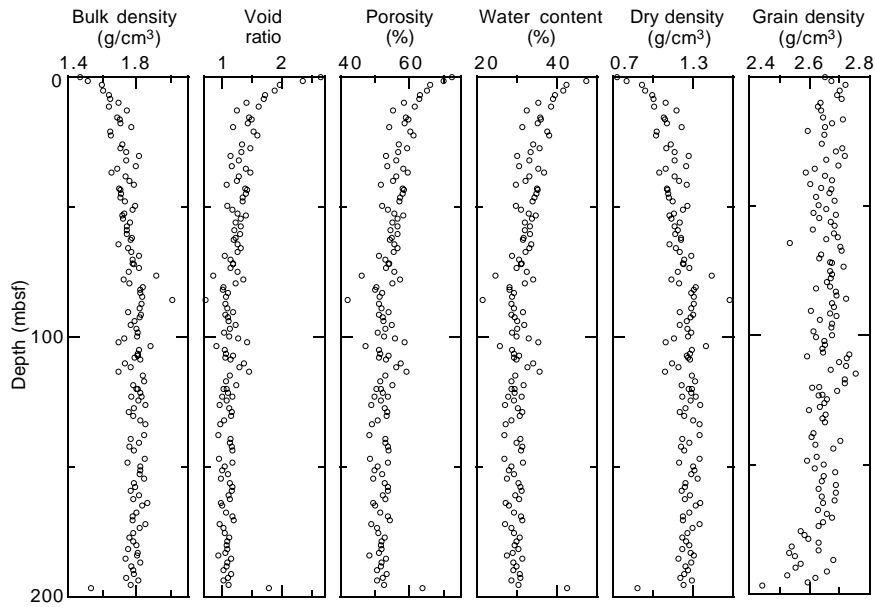


Figure 19. Index property data from Hole 1017B.

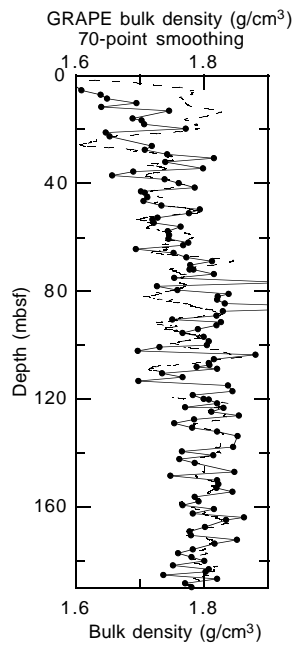


Figure 20. Hole 1017B bulk density (line with solid circles indicating each index property measurement) with GRAPE bulk density smoothed with a 70-point running average (dashed line).

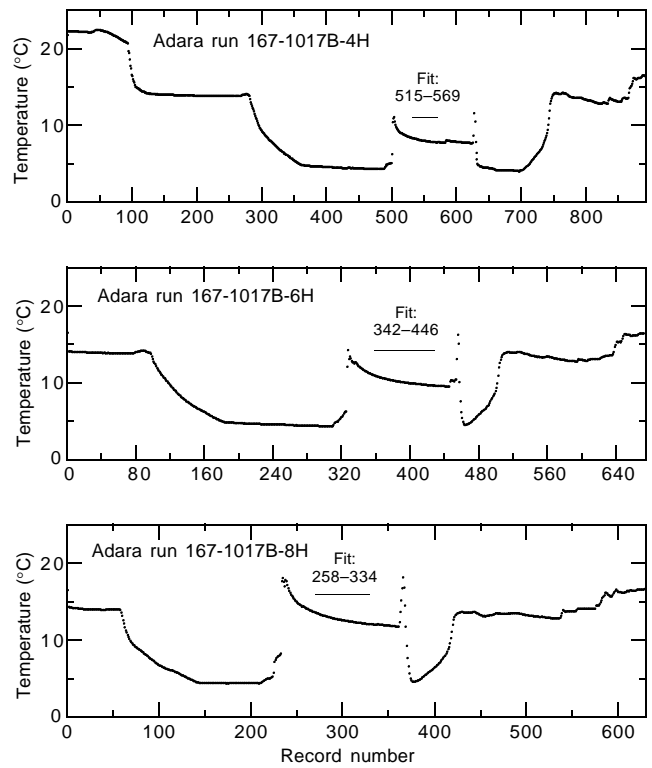


Figure 21. Hole 1017B downhole temperature vs. record number (5-s recording frequency) for each measurement run, showing the intervals fitted to determine the downhole temperature.

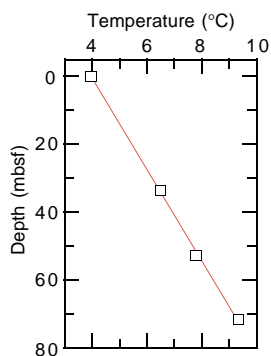


Figure 22. Downhole temperature gradient from Hole 1017B.

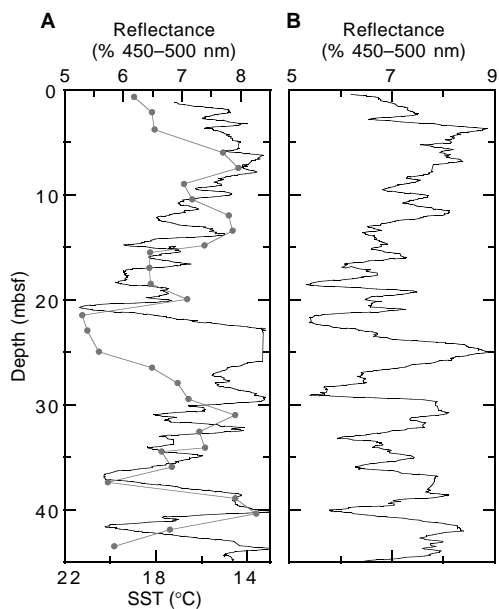


Figure 23. **A.** Average percent color reflectance for the 450–500-nm band (solid line) and estimated SST vs. depth (line with data points) for Hole 1017B. **B.** Average percent reflectance for the same band vs. depth (mbsf) in Hole 1017C.

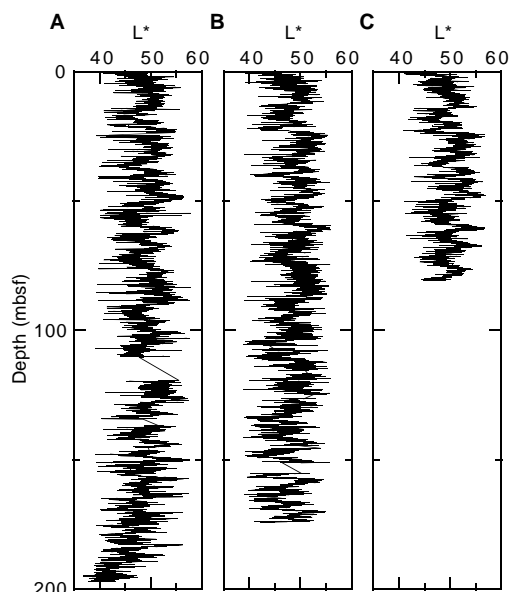


Figure 24. Digital color video data for color CIELAB L* from Holes (A) 1017B, (B) 1017C, and (C) 1017D. Data were decimated at 2-cm intervals.

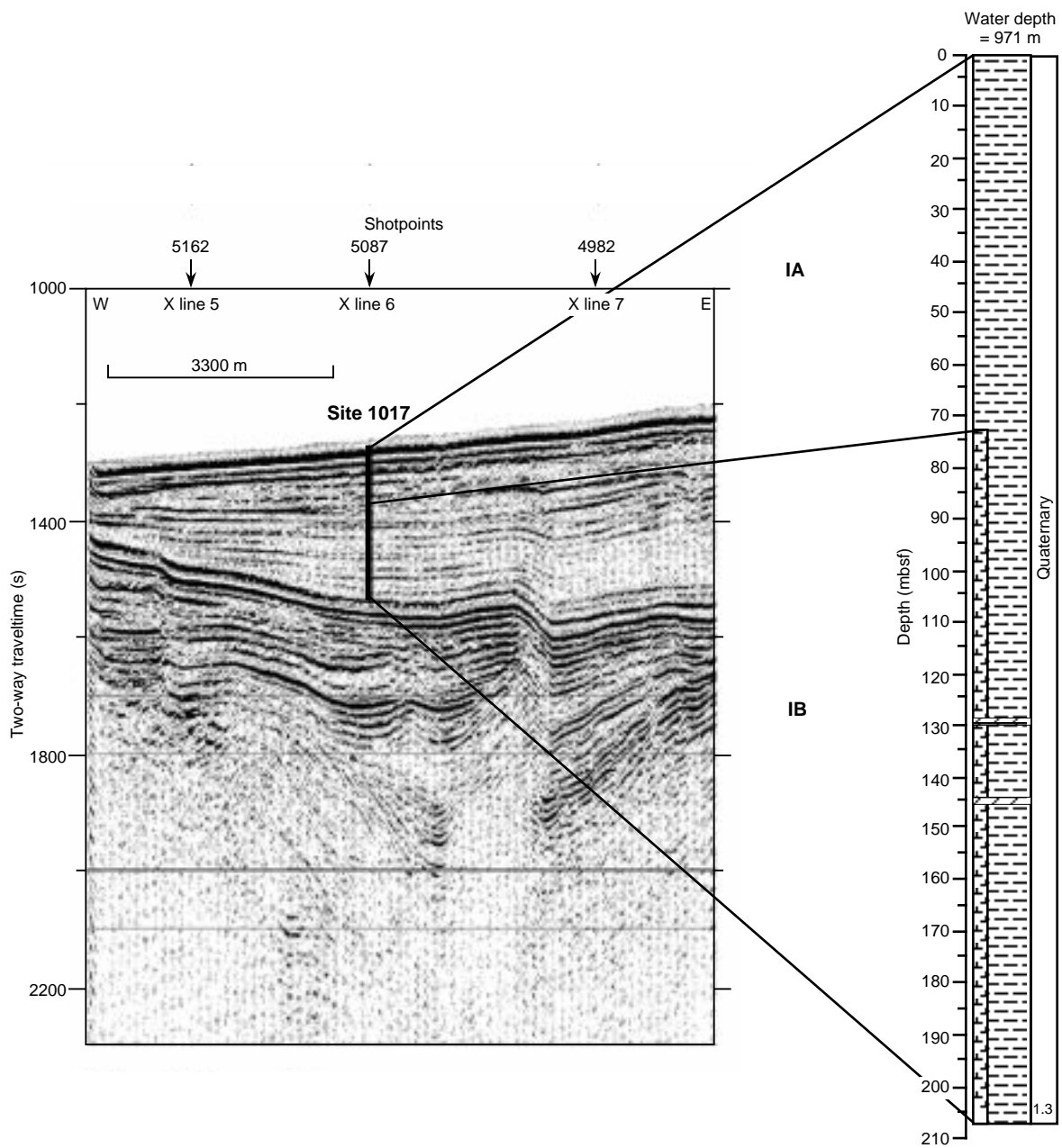


Figure 25. Comparison of the lithostratigraphic column at Site 1017 and a seismic reflection profile through the site (Line EW9504 CA9-8; Lyle et al., 1995a, 1995b). Ties are calculated from shipboard velocity measurements (see “Physical Properties” section, this chapter). On y-axis, (s) = milliseconds.